ACS EARTH AND SPACE CHEMISTRY
http://pubs.acs.org/journal/aesccq
Article

Hourly Measurements of Organic Molecular Markers in Urban Shanghai, China: Primary Organic Aerosol Source Identification and Observation of Cooking Aerosol Aging

Qiongqiong Wang, Xiao He, Min Zhou, Dan Dan Huang, Liping Qiao, Shuhui Zhu, Ying-ge Ma, Hong-li Wang, Li Li, Cheng Huang,* X. H. Hilda Huang, Wen Xu, Douglas Worsnop, Allen H. Goldstein, Hai Guo, and Jian Zhen Yu*

Cite This: *ACS Earth Space Chem.* 2020, 4, 1670–1685
Read Online

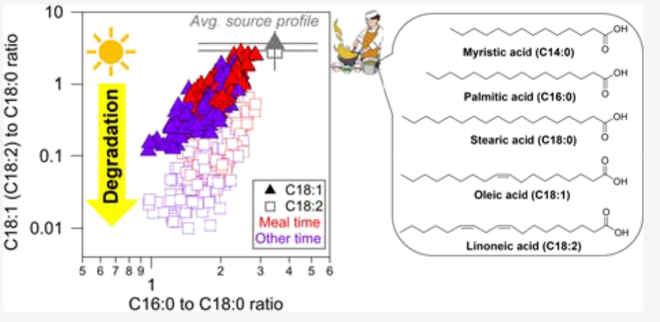

ABSTRACT: Molecular markers in ambient organic aerosol (OA) provide highly specific source information. Their traditional quantification is based on offline analysis of filter samples, and the coarse time resolution and labor-intensive nature hugely limit the utility of the tracer data. In this study, hourly organic molecular markers in fine particulate matter were measured using a recently commercialized thermal desorption aerosol gas chromatography–mass spectrometry (TAG) technique at an urban location in Shanghai, China during a three-week campaign from 9 November to 3 December, 2018. Selected primary OA molecular markers, including anhydrosugars, fatty acids, aromatic acids, and polycyclic aromatic hydrocarbons (PAHs), were examined in detail. Their diurnal variations showed characteristic features representing the corresponding emission source activities. For example, stearic acid showed a clear peak around 7 pm, in accordance with the enhanced cooking activities during mealtime. Diagnostic ratios of related makers of different reactivities provided unique information in uncovering the source information and tracking evolution of the OA in the atmosphere, for example, ratios of levoglucosan to its isomers and K^+ identified crop residue burning as the major form of biomass burning (BB). Ratios of unsaturated and saturated fatty acids gave unambiguous indication of atmospheric degradation of unsaturated fatty acids after emissions. Oleic acid to stearic acid ratios in ambient data (0.83 ± 0.54) were lower than those in the source profiles (1.2–6.5). Furthermore, the oleic acid to stearic acid ratio was found to be highly correlated with O/C ratios (R_p: −0.66), suggesting the possible utility of oleic acid as a model compound to examine the heterogeneous reaction of cooking-related OA. PAH ratio–ratio plots helped identify varying influences of major combustion sources associated with air masses of different origins, revealing that BB and coal combustion were dominant under the influence of long-range transport air mass, while vehicle emissions were dominant under local/median-range air mass influence. This study demonstrated the utility of high time-resolution organic markers in capturing the dynamic change of source emissions and atmospheric aging, providing observational evidence to support their use in source apportionment.

KEYWORDS: *organic molecular markers, primary organic aerosols, thermal desorption aerosol gas chromatography–mass spectrometry, source identification, atmospheric aging, cooking aerosol, biomass burning*

■ INTRODUCTION

Organic aerosol (OA) is an important fraction of airborne fine particulate matter ($PM_{2.5}$, particles with an aerodynamic diameter less than 2.5 μm), contributing to 20–90% of the total $PM_{2.5}$ mass.[1] OA is typically divided into primary OA (POA) and secondary OA (SOA). POA is directly emitted to the atmosphere by a variety of sources, while SOA is secondarily formed in the atmosphere. Compared with inorganic components (i.e., sulfate, nitrate, and ammonium), OA is considerably more complex in their composition. OA contains tens of thousands of individual compounds,[2] some of which are highly source specific or indicative of secondary transformation of certain precursors. Thus, these organic molecular markers are highly valuable in serving as source tracers for the apportionment of source contributions and formation processes of OA and hence help formulate effective control measures.[3−5]

Received: July 28, 2020
Revised: August 6, 2020
Accepted: August 11, 2020
Published: August 11, 2020

https://dx.doi.org/10.1021/acsearthspacechem.0c00205
ACS Earth Space Chem. 2020, 4, 1670–1685

Fresh POA, upon emission, is diluted by background air and subjected to atmospheric oxidation. The particle-phase organics can be oxidized via heterogeneous uptake of atmospheric oxidants such as ozone, OH, and NO_3 radicals. Their concentrations measured at receptor sites are subjected to combined influences from source emissions, atmospheric dilution, and photochemical oxidation. Degradation of the organic markers in the atmosphere is a major concern when using them as source tracers. Previous studies examining the atmospheric stability of organic markers are mainly based on laboratory studies.[6,7] For example, the ozonolysis mechanism and kinetics of oleic acid have been extensively studied in chamber experiments.[8−10] These laboratory studies report that assuming the reaction rate of pure oleic acid particles, oleic acid would have a lifetime of minutes in the atmosphere, and the lifetime increases to tens of hours when the reaction occurs in a liquid/solid matrix.[10] In comparison, field studies had observed oleic acid in aged aerosols (2−3 days), e.g., ref 11. Clearly, the aging of POA markers under ambient atmospheric conditions is still far from being properly understood, and highly time-resolved observations will help bridge this knowledge gap.

Current understanding of OA in the ambient atmosphere is mainly based on offline analysis of filter samples and online measurements by aerosol mass spectrometers. Online mass spectrometers, such as aerosol mass spectrometry (AMS)[12] and single-particle mass spectrometry,[13] provide high time-resolution data of ion fragments down to several minutes, thus having the advantage in capturing the dynamic change of OA. These online measurements have greatly advanced our understanding of the atmospheric chemistry of OA and their role in affecting climate.[14] However, these instruments do not identify individual organic compounds at the molecular level. Instead, fragment ions are monitored, and a given ion could be associated with multiple organic compounds, thereby complicating their use in tracking sources. On the other hand, offline analysis of filter samples quantifies individual source-specific molecular markers, providing distinct molecular links to sources. Such offline data, commonly collected over an integrated time period of a day, offer no information on the diel dynamic variation of the OA. Short-term sampling schedules, e.g., 3 to 12 h, have also been explored with the filter-based chemical characterization approach to examine the diurnal variation of OA.[15−22] However, the laborious nature of such an approach makes it impractical to have a long temporal coverage or reliably capture episodic events.

The development of thermal desorption aerosol gas chromatography−mass spectrometry (TAG)[23−26] enables hourly monitoring of organic molecular markers. The first version of TAG was reported in 2006.[23] Several significant improvements of the system have been made subsequently, including an automated high temperature valveless injection system,[24] an autoinjection system capable of introducing internal standards (ISs) on each sample,[25] and an online derivatization system for measuring both polar and nonpolar organic species.[26] These new instrument features have largely improved the identification and quantification of organic species. The hourly resolution organic marker data from TAG have been demonstrated to be effective in apportioning OA sources in California[27,28] and sources of black carbon in downtown Pittsburgh.[25] The high time-resolution data are also expected to provide information for examining the evolution of OA in the real atmospheric environment.[29]

In this study, we deployed a commercial TAG instrument from Aerodyne Research Inc. at an urban location in Shanghai, China, in a consecutive three-week field campaign from 9 November to 3 December, 2018, along with an array of other online aerosol instruments. A set of 72 individual organic compounds, including POA and SOA source tracers, were quantified. The examination of SOA tracers measured in this campaign is reported elsewhere by He et al.[30] The objective of this work is to demonstrate the use of hourly organic molecular markers for identifying POA sources and tracking their aging process in a typical urban area. The results provide observational evidence and insights for improved quantitative understanding of POA sources and atmospheric processing.

■ METHOD

Chemicals. Chemical standards and deuterium-labeled ISs were purchased from CDN Isotopes (Point-Claire, Quebec, Canada), Cambridge Isotope Laboratories (Andover, MA), and Sigma-Aldrich Chemicals (Bornem, Belgium) and prepared in 1:4 ACN and CH_2Cl_2. The deuterated ISs used in this study included levoglucosan-d_7, glucose-d_7, $C_{16}D_{34}$, $C_{20}D_{42}$, $C_{24}D_{50}$, $C_{28}D_{58}$, $C_{36}D_{74}$, phenanthren acid-d_{10}, chrysene-d_{12}, perylene-d_{12}, benzo[ghi]perylene-d_{12}, succinic acid-d_4, adipic acid-d_{10}, azelaic acid-d_{14}, citric acid-d_4, myristic acid-d_{27}, palmitic acid-d_{31}, stearic acid-d_{35}, cholesterol-d_6, and phthalic acid-d_4. N-methyl-N-(trimethylsilyl) trifluoroacetamide (MSTFA, Sigma-Aldrich) was used as a derivatization agent for analytes containing −OH and −COOH groups.

Sampling and TAG Measurement. The field measurements were conducted at Shanghai Academy of Environmental Sciences (SAES, 31.17°N, 121.43°E), located in the southwest of the central urban area of Shanghai, China. The site is influenced by various typical urban emission sources (e.g., vehicular emissions, cooking, etc.) as well as pollution from regional transport (e.g., coal combustion, biomass burning (BB), etc.).[31] The sampling inlet was located on the 8th floor of the building (∼25 m above ground level).

Hourly organic molecular markers were measured from 9 November to 3 December, 2018 using a TAG module (Aerodyne Research Inc., https://www.aerodyne.com/wp-content/themes/aerodyne/fs/TAG_0.pdf) coupled with a gas chromatograph/mass spectrometer (GC/MS) (Agilent GC 6890 N/MSD 5973 N). Figure S1 shows the schematic diagram of the TAG system. This version of TAG employs a multichannel carbon denuder to remove gaseous organics, a 9-jet impactor collection, a thermal desorption cell (CTD),[23] an auto-injection system for in-situ calibration and injection of ISs onto every ambient sample, and an in-situ derivatization system delivering MSTFA for the silylation of polar organic species containing −OH and −COOH functionalities. The sampling flow rate was 8 L/min. The instrument component details were described by Isaacman et al.[26]

Goldstein and co-workers have proved that the TAG system is capable of measuring hundreds of organic species.[23,26] In this work, we focus on a subset of source-specific POA markers. The detailed description of the working principle of TAG can be found in previous studies.[23,26,32] Only the sampling and operation relevant to this study are described here. During sampling, ambient air was drawn through a $PM_{2.5}$ cyclone (10 L/min, 2.5 μm size cut, URG-2000-30EN) followed by a multichannel carbon denuder,[32] and then, particles in the sampled air were collected on the CTD maintained at 30 °C. The sampling duration was 60 min followed by a 32-min

https://dx.doi.org/10.1021/acsearthspacechem.0c00205
ACS Earth Space Chem. 2020, 4, 1670−1685

Table 1. Statistics of Hourly Concentrations of TAG-Measured Organic Species and Other $PM_{2.5}$ Components During the Campaign (N = 269)

compounds	average	SD	min.	max.	recovery	quantification IS
TAG measured molecular species (ng/m^3)						
Myristic acid[a]	2.47	1.36	0.73	11.0		Myristic acid-d_{27}
Palmitic acid	49	42.6	3.8	268.1	88.4 ± 2.4	Palmitic acid-d_{31}
Stearic acid	24.5	18.3	2.72	113.9	75.6 ± 3.2	Stearic acid-d_{35}
Oleic acid	25.4	35.9	0.65	219.1	111.8 ± 7.7	Stearic acid-d_{35}
Linoleic acid[b]	4.57	7.72	BD[d]	56		Stearic acid-d_{35}
Galactosan	1.13	1.2	0.05	9.19	79.2 ± 3.1	Levoglucosan-d_7
Mannosan	1.53	1.5	0.05	8.9	74.6 ± 3.1	Levoglucosan-d_7
Levoglucosan	45.9	39.2	1.02	238.4	116.2 ± 3.4	Levoglucosan-d_7
Mannitol	3.35	1.93	0.74	13.8	84.4 ± 7.0	Glucose-d_7
Glucose	8.61	5.39	1.6	36	96.0 ± 5.4	Glucose-d_7
Sucrose	52.9	49.4	7.75	362.9	94.7 ± 8.2	Glucose-d_7
3-hydroxybenzoic acid	0.47	0.34	0.07	2.23	94.9 ± 10.8	Phthalic acid-d_4
4-hydroxybenzoic acid	0.61	0.51	2.23	3.74	81.6 ± 4.5	Phthalic acid-d_4
Isophthalic acid	0.49	0.33	0.03	2.15	77.0 ± 9.1	Phthalic acid-d_4
Terephthalic acid	5.22	4.61	BD	34.9	67.3 ± 6.8	Phthalic acid-d_4
Phthalic acid	9.13	10.3	BD	65.9	83.5 ± 3.9	Phthalic acid-d_4
Nonanoic acid[c]	0.22	0.22	BD	1.50		Azelaic acid-d_{14}
9-oxononanoic acid[c]	3.48	2.36	0.31	14.1		Azelaic acid-d_{14}
Azelaic acid	6.06	4.44	0.20	27.1	65.1 ± 7.8	Azelaic acid-d_{14}
Fluoranthene	0.35	0.26	0.02	1.51	85.1 ± 1.2	Phenanthrene-d_{10}
Pyrene	0.34	0.23	0.03	1.48	85.3 ± 1.1	Phenanthrene-d_{10}
Chrysene (CHR)	0.18	0.14	0.06	1.19	80.4 ± 1.4	Chrysene-d_{12}
Benz[a]anthracene (BaA)	0.34	0.29	BD	1.85	87.7 ± 1.7	Chrysene-d_{12}
Benzo[b]fluoranthene (BbF)	0.19	0.17	BD	1.2	73.1 ± 2.3	Perylene-d_{12}
Benzo[k]fluoranthene (BkF)	0.41	0.4	0.05	2.69	77.3 ± 1.6	Perylene-d_{12}
Benzo[e]pyrene (BeP)[e]	0.36	0.32	0.02	2.18		Perylene-d_{12}
Benzo[a]pyrene (BaP)[e]	0.48	0.56	0.03	3.92		Perylene-d_{12}
Perlyene[e]	0.23	0.24	BD	2.14		Perylene-d_{12}
Indeno[1,2,3-cd]pyrene (IcdP)	0.35	0.32	0.05	2.43	102.6 ± 2.9	Benzo[ghi]perylene-d_{12}
Benzo[ghi]perylene (BghiP)	0.21	0.22	BD	1.66	82.6 ± 1.0	Benzo[ghi]perylene-d_{12}
$PM_{2.5}$ and major components (μg/m^3)						
$PM_{2.5}$	47.4	33.7	8	154		
Chloride	0.75	0.45	0.06	2.92		
Sulfate	6.28	3.30	1.15	19.5		
Nitrate	12.9	12.8	0.77	52.6		
Ammonium	6.19	5.08	0.50	22.8		
K^+	0.13	0.08	0.02	0.47		
BC	2.35	1.66	0.21	10.7		
As	0.003	0.002	0.0001	0.01		
OA (PM_1)	14.1	11.1	1.5	60.8		

[a]Quantified using palmitic acid as the surrogate. [b]Quantified using oleic acid as the surrogate. [c]Quantified using azelaic acid as the surrogate. [d]Below detection limit. [e]Quantified using BbF as the surrogate, using 0.1, 0.05, and 0.04 times of the response factor for BbF, which was determined by comparing the calibration curves of BeP, BaP, perylene, and BbF using standards from the offline thermal desorption GC/MS method.

thermal desorption step. Before thermal desorption, 5 μL of IS mixtures were added to the CTD. A two-step thermal desorption was adopted to desorb and transfer samples from the CTD to the GC column. The CTD was set and held at 45 °C for 2 min, increased to 330 °C in 6 min, and held at 330 °C for 12 min. Samples were desorbed from the CTD and in the same time underwent in-situ derivatization under a helium stream saturated with MSTFA (10 sccm He and 40 sccm MSTFA for 6 min followed by 16 sccm He and 64 sccm MSTFA for 6 min and lastly 100 sccm pure He for 8 min). The desorbed analytes were then re-concentrated onto the focusing trap held at 45 °C. Then, the focusing trap was heated to 315 °C, pressurized to 42 psi, and backflushed with a helium flow at 4 sccm through the valveless manifold, transferring the analytes onto the head of the GC column (DB-5MS, 30 m × 0.25 mm × 0.25 μm). This step took 12 min. The temperature program in the GC analysis was initially at 45 °C for 5 min, ramped at 5 °C /min to 200 °C and held for 2 min, and then ramped at 10 °C /min to 300 °C and held for 12 min. Excluding the time (32 min) the steps spent on derivatization and thermal desorption, the GC/MS analysis of each sample took 60 min, and this was concurrent with collecting the next ambient sample. In order to compare with other hourly online instruments, TAG only collected hourly samples every odd hour, and no samples were collected for the even hours.

https://dx.doi.org/10.1021/acsearthspacechem.0c00205
ACS Earth Space Chem. 2020, 4, 1670−1685

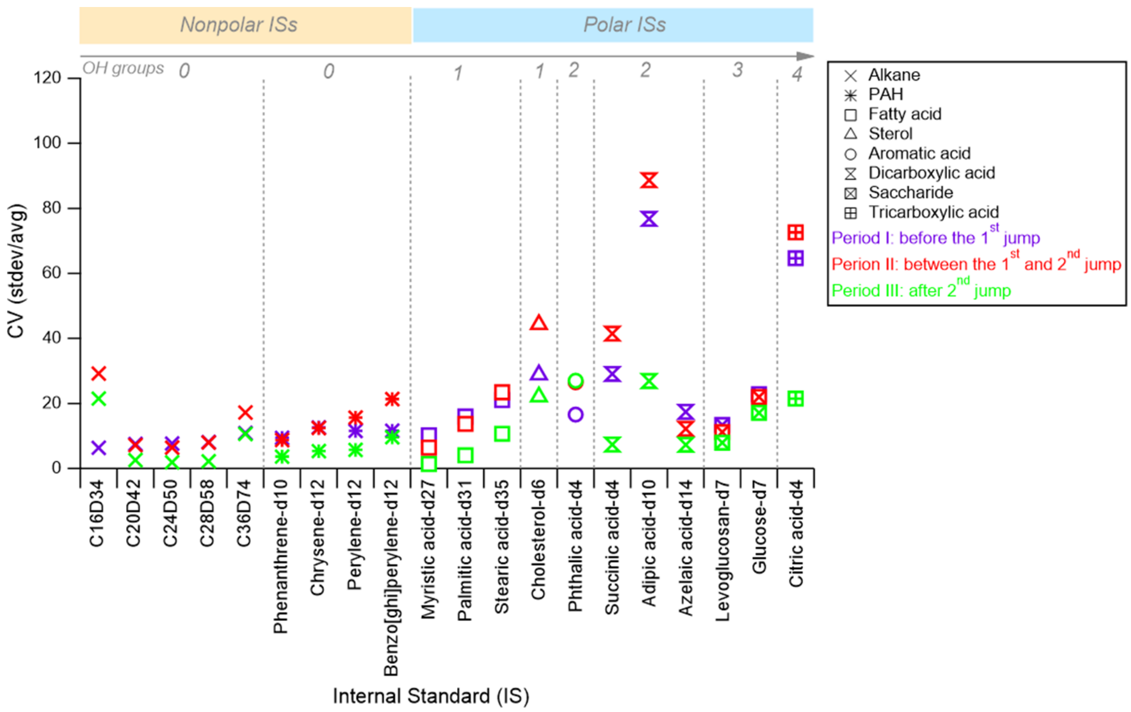

Figure 1. CV of the peak area of each deuterated IS corresponding to three subperiods (period I: before the 1st jump on 20 November, period II: between the 1st and 2nd jump, and period III: after 2nd jump on 2 December).

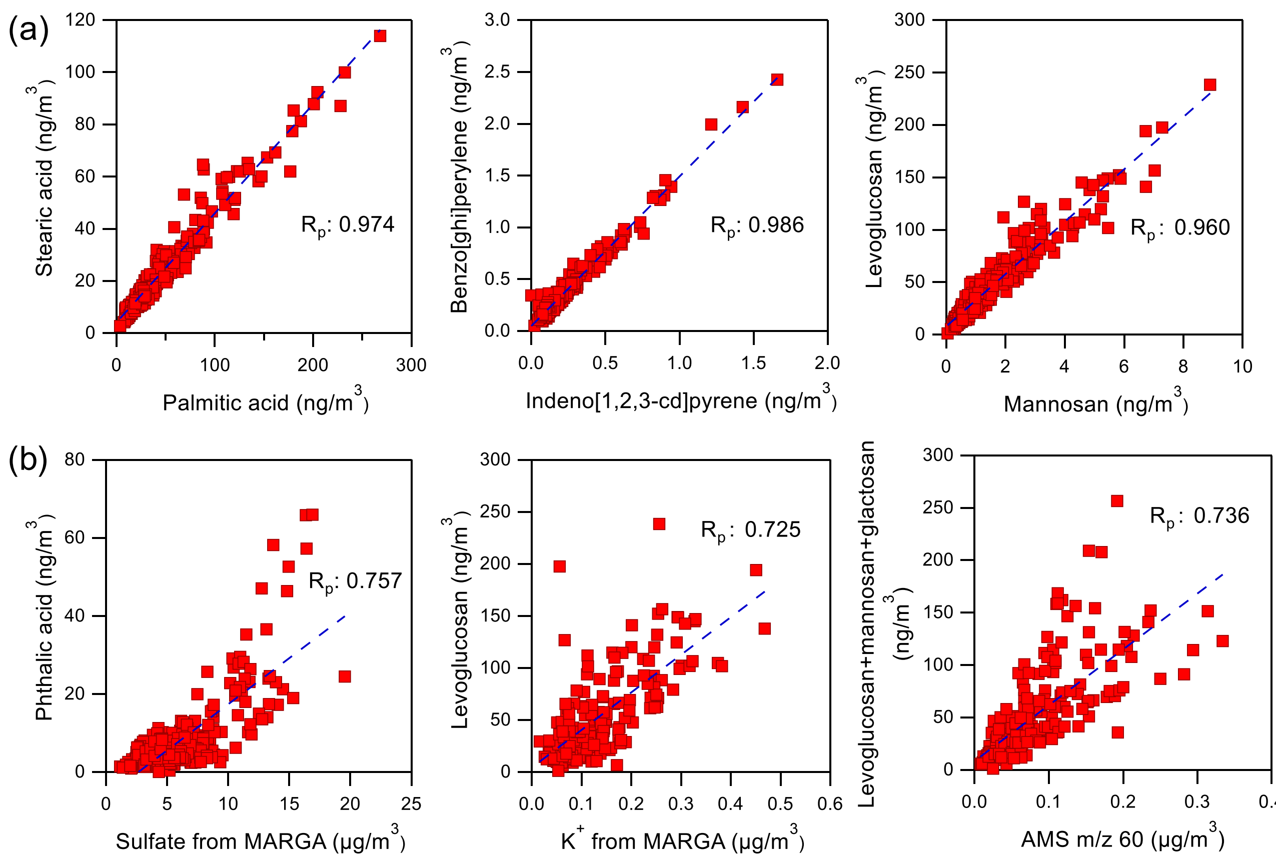

Figure 2. (a) Scatter correlation plots for isometric/homologue species obtained by TAG. (b) Three examples of TAG-measured organic markers versus related-source indicative species by other instruments, including phthalic acid versus sulfate by MARGA, levoglucosan versus K^+ by MARGA, and anhydrosugars versus *m/z* 60 by AMS.

The list of target organic molecular markers discussed in this work is provided in Table 1. Compound identification was carried out through comparing retention times and mass spectra with those of authentic standards. Quantification was

https://dx.doi.org/10.1021/acsearthspacechem.0c00205
ACS Earth Space Chem. 2020, 4, 1670−1685

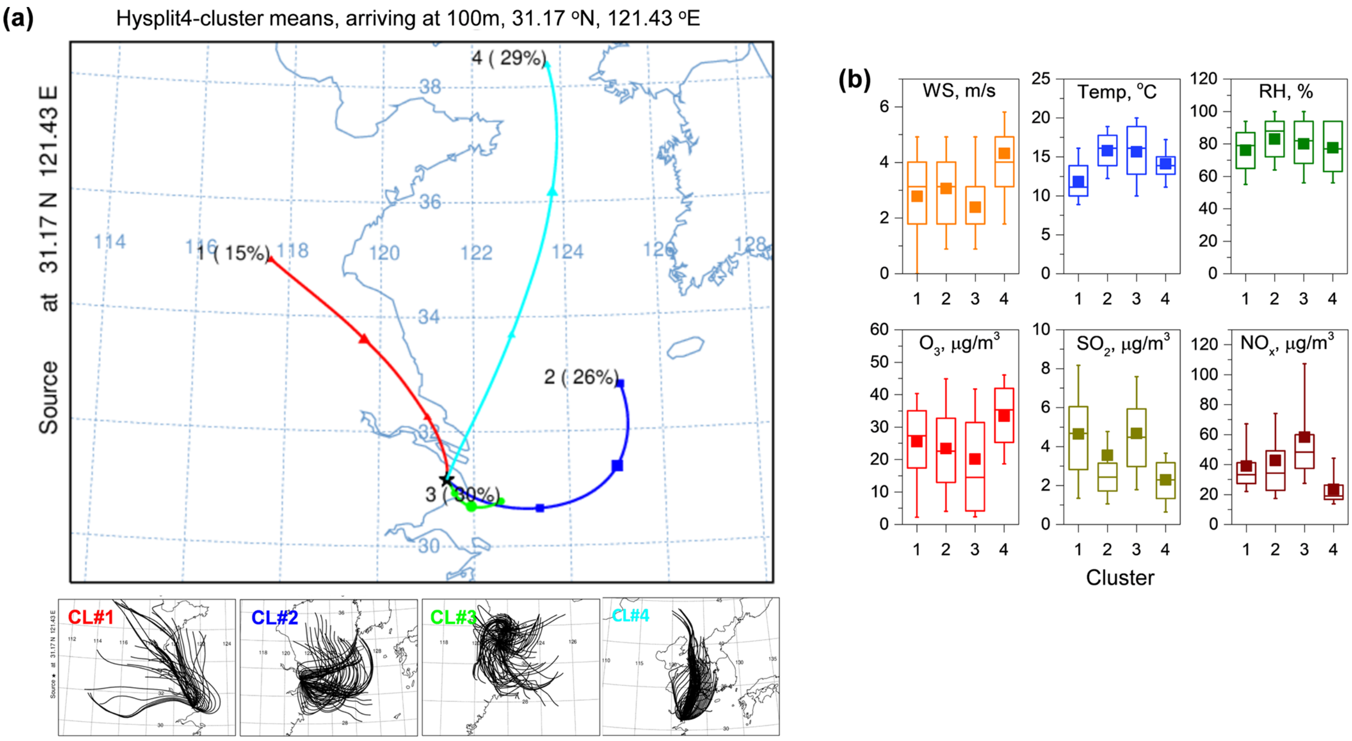

Figure 3. (a) Distribution of the 36 h backward trajectory clusters arriving at the SAES site at 100 m above the ground level from 9 Nov. to Dec. 3, 2018. Individual trajectories in each cluster are shown in the bottom panel. (b) Statistic summary in box plots of meteorological parameters and gas pollutant concentrations in each cluster (squares and solid lines correspond to mean and median values, respectively; box indicates the 25th and 75th percentile, and whiskers are the 10th and 90th percentile).

done by introducing liquid standard mixtures of known amounts into the CTD. Calibration curves were built by plotting the peak area ratios of each standard to their respective IS versus the amount (per injection) of the target compound in the standard mixtures. The correlation coefficients (R_p) of calibration curves were in the range of 0.92−1.00. For compounds without authentic standards and compounds whose authentic standards are not included in current standard mixtures, their identification was performed by comparing their mass spectra with the National Institute of Standards and Technology (NIST) library and their quantification using surrogate standards as specified in Table 1. Chromatogram peak fitting and integration was done using Igor-based (version 6.37) TERN software (version 2_2_1).[33] The peaks were fitted with the residual less than 10%.

Quality Assurance/Quality Control of TAG Measurements. Details about the quality assurance/quality control are provided in Text S1. In brief, one blank sample was collected every 2 days of consecutive sampling, and one standard mixture was injected once per week to monitor the GC/MS condition. In total, 285 samples were obtained, including 11 blank samples and 5 standard mixture samples. The blank samples were collected with the entire sampling flow bypassing the denuder and the CTD and going directly to the pump exhaust (Figure S1), therefore reflecting the residue remaining with the TAG. The blank samples showed little contamination for the target species listed in Table 1. However, relatively high blank levels were observed with light and heavy *n*-alkanes ($<C_{18}$ and C_{33}−C_{37}) and a few polar organics (e.g., vanillic acid, syringic acid, and cholesterol). These organic compounds were excluded from our target analyte list.

The sample-to-sample variation of the deuterated ISs serves as a measure of the precision of the measurement of the TAG system. The peak area time series of the deuterated ISs reveal two occasions of concurrent jumps followed by immediate stabilization at the newer level (Figure S2). The first jump occurred at noon time on November 20 and the second one on December 2. Our analysis indicates that these sudden changes in IS responses were most likely related to the change in the matrix (Text S1.2). The first jump coincided with the rapid decrease of PM mass (13:00−15:00 on November 20) right before a rain event. The second elevation of the IS signals (11:00−13:00 on December 2) was derived from the influence of MSTFA refill. For each subperiod before and between the jumps, we calculated the coefficients of variation (CVs) of the IS peak area signals, which represent quantification consistency for samples of a similar matrix. In another words, they could be considered as within-matrix variations. The overall CVs, on the other hand, reflect the between-matrix variations. The within-matrix CV values are summarized in Table S1 and shown in Figure 1. As one would expect, the within-matrix CVs are notably lower than the between-matrix CVs for all compound groups. For example, the within matrix CV for chrysene-d_{12} was in the range of 5−13%, while the overall CV was 17%; the within matrix CV for palmitic acid-d_{11} was in the range of 4−16%, while the overall CV was 28%.

Internal data consistency was checked through examining correlations of isomeric/homologue species measured by TAG. The results for levoglucosan versus mannosan, indeno[1,2,3-cd]pyrene versus benzo[ghi]perylene, and palmitic acid versus stearic acid are shown in Figure 2a. Strong correlations were observed for related pairs of markers (R_p: 0.96−0.99). Also, good correlations were observed between TAG-measured

https://dx.doi.org/10.1021/acsearthspacechem.0c00205
ACS Earth Space Chem. 2020, 4, 1670−1685

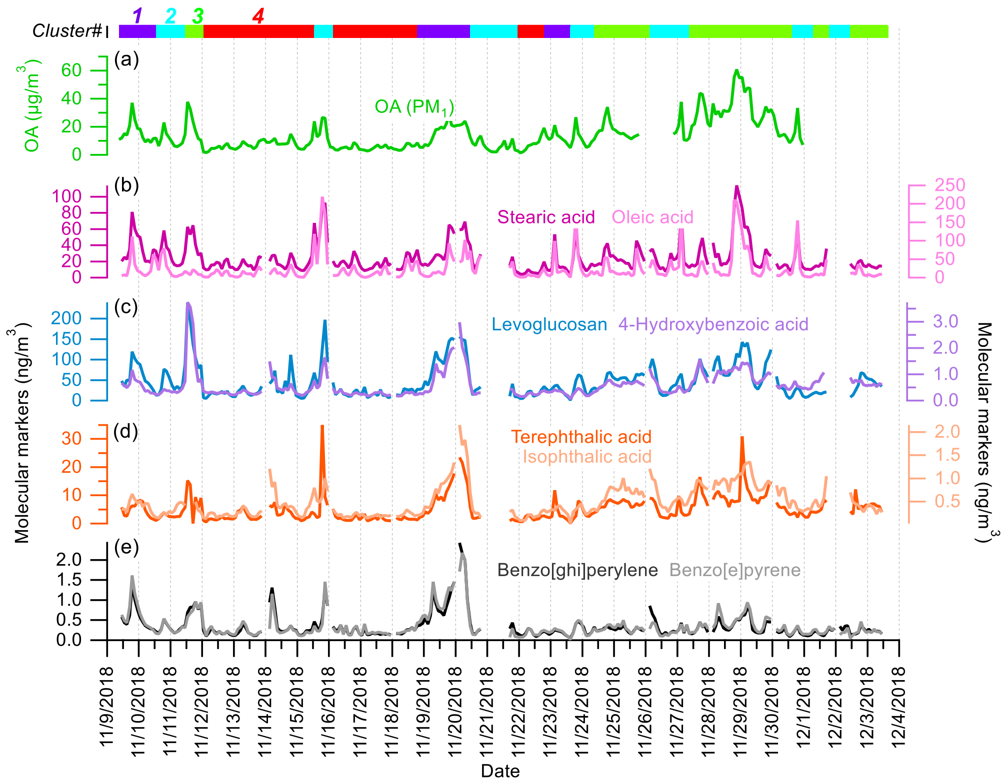

Figure 4. Campaign-wide temporal variations of (a) total OA (PM_1) and select molecular markers including (b) stearic and oleic acid, (c) levoglucosan and 4-hydroxybenzoic acid, (d) terephthalic and isophthalic acid, and (e) benzo[ghi]perylene and benzo[e]pyrene.

organic markers with the related-source indicative species from other instruments, such as levoglucosan by TAG versus K^+ by MARGA, phthalic acid by TAG versus sulfate by MARGA, and sum of the three isomeric anhydrosugars by TAG versus m/z 60 fragment by AMS, with R_p in the range of 0.73−0.76 (Figure 2b). The results lend credence to the TAG data quality in this study.

The variation of the TAG sampling flow during the whole campaign is shown in Figure S6. The sampling flow rate was 7.4 L/min at the beginning of the campaign and decreased to 4.7 L/min at the end of the campaign, caused by accumulation of particles partially blocking the 9-jet impactor. The reduction in the sampling flow rate would lead to the shift of PM size cut to a larger size. For example, at 10 L/min, the cyclone cut point is 2.5 μm; when the flow rate decreases to 5 L/min, the cut point increases to 4 μm.

Other Measurements. The hourly meteorological parameters (temperature, relative humidity, wind speed, and wind direction) and gas pollutants (NO_x, SO_2, CO, and O_3) were measured at the site. Hourly $PM_{2.5}$ mass was measured with an online beta attenuation particulate monitor (FH 72 C14 series, Thermo Fisher Scientific), water-soluble inorganic ions (SO_4^{2-}, NO_3^-, NH_4^+, Cl^-, and K^+) with an online Monitor for AeRosols and Gases in the ambient Air (MARGA, Model ADI 2080, Applikon Analytical B.V.), black carbon (BC) with an aethalometer (AE22, Magee Scientific Co.), and elemental species (K, S, Ca, and As) with an ambient continuous multimetal monitor (Xact 625, Cooper Environmental Services, Tigard, OR, USA). Instrument details at this site have been described elsewhere.[31,34] Total OA concentrations, mass fragmentation ions of m/z 60, and atomic oxygen-to-carbon (O/C) ratios in PM_1 were obtained using AMS (Aerodyne Research Inc., Billerica, Massachusetts, USA) and averaged to hourly data for comparison with the TAG data.

For data validation, SO_4^{2-} and K^+ measured by MARGA were compared with total S and K measured by Xact, respectively (Figure S7). AMS measured PM_1 components, including sulfate, nitrate, ammonium, and chloride, were also compared with MARGA measurements (Figure S8). Good agreement was observed across different instruments, as evidenced by high correlations (R_p: 0.80−0.92).

RESULTS AND DISCUSSION

Backward Trajectory Clustering Analysis. Backward trajectory analysis was performed using the Hybrid Single-Particle Lagrangian Integrated Trajectory model (http://www.arl.noaa.gov/ready/hysplit4.html). The Global Data Assimilation System 0.5° global meteorological data were utilized to calculate the 36 h duration backward trajectories arriving at an altitude of 100 and 300 m above the ground level over the site. The trajectories were then clustered according to the similarity in spatial distribution.

The solutions with 3, 4, and 5 clusters were initially examined. An optimal solution of four clusters was determined based on the change in total spatial variance (Figure S9). The four-cluster solution with the arrival height of 300 m was similar to that of 100 m and thus not further discussed. Figure 3 shows the distribution of the cluster means and diel variations of meteorological conditions and gas pollutants in each cluster for the four-cluster solution at 100 m arrival height. Their time series are shown in Figure S10. Briefly, cluster #1 (CL#1), accounting for 15% of the samples, originated from the northern continental area, passing through the agriculture areas of Shandong, Henan, and Jiangsu provinces. The lower temperature associated with this cluster

https://dx.doi.org/10.1021/acsearthspacechem.0c00205
ACS Earth Space Chem. 2020, 4, 1670−1685

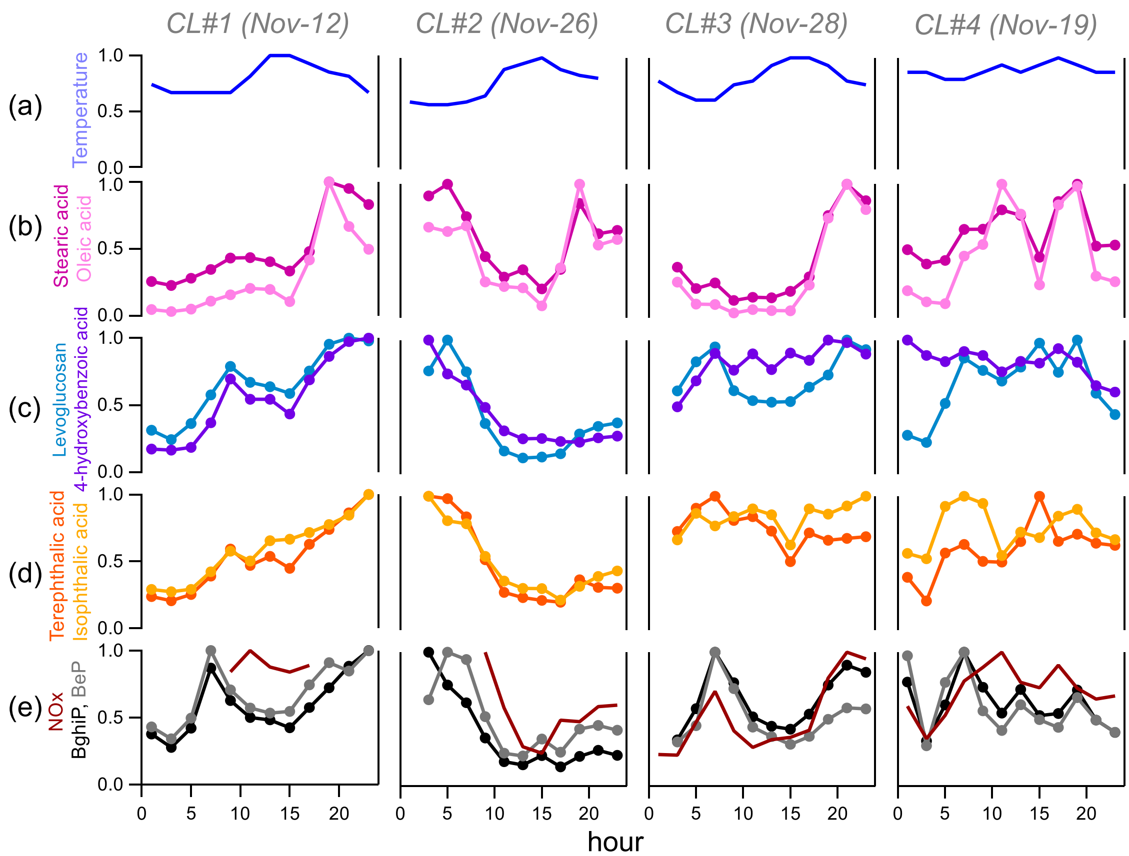

Figure 5. Diurnal variations on selected days under each cluster for (a) temperature and POA markers including (b) stearic and oleic acid, (c) levoglucosan and 4-hydroxybenzoic acid, (d) terephthalic and isophthalic acid, and (e) benzo[ghi]perylene and benzo[e]pyrene. The POA markers within each day are normalized against their respective highest concentration. The diurnal variation of NO_x is also shown in (e).

is consistent with this geographic origin. Cluster #2 (CL#2), consisting of 26% of the samples, represented air mass from the ocean to the east/southeast. Cluster #3 (CL#3), accounting for 30%, was characterized by trajectories circulating around the local area and associated with the lowest wind speed observed. Cluster #4 (CL#4), 29% of the samples, mainly represented northeastern oceanic air mass. CL#4 had the longest trajectory length and was associated with the highest wind speed and O_3 concentrations observed. CL#3 was associated with the highest NO_x concentration (Figure 3b), confirming its local air mass origin. SO_2 was appreciably higher in samples associated with CL#1 and CL#3 than those with CL#2 and CL#4, reflecting that coal combustion influenced both air transported from long-range over the continent[35] and from local sources.

General Characteristics of OA and Characteristic Molecular Markers. Hourly $PM_{2.5}$ ranged from 8 to 154 (47.4 ± 33.7) $\mu g/m^3$, and total PM_1 OA concentrations ranged from 1.5−60.8 (14.1 ± 11.1) $\mu g/m^3$, indicating large variations of PM pollution experienced during the field campaign. Figure 4 displays the time series of total OA and selected POA markers, showing periods of relative constant concentrations interspersed with spikes lasting hours. Table 1 provides a statistical summary of the concentrations of measured organic species and other aerosol components during the campaign. Both the minimum and maximum concentrations reported in Table 1 and the time series shown in Figure 4 showed larger sample-to-sample variation in POA marker concentrations, and the more reactive organic markers had a more prominent variation than the less reactive ones. For example, the maximum hourly concentration (219 ng/m^3) of oleic acid was 337 times that of the minimum hourly concentration (0.65 ng/m^3), in comparison with 42 times between the maximum (114 ng/m^3) and the minimum concentrations (2.7 ng/m^3) for stearic acid. This molecule-specific variation information could be useful in observing the aging of aerosols from a source, which will be discussed in a later section.

The diurnal variation of measured species at an ambient site is a combined effect of input from the emission sources, loss due to degradation/deposition, and dilution/compaction from atmospheric boundary layer height variation. In this study, we examined the diurnal variation of temperature to help indicate the variation of boundary layer height. In general, under CL#4, temperature remained fairly constant in the diel cycle, while under CL#2&3, a more obvious diurnal cycle of temperature was observed, indicating larger variation of boundary layer height in the diel cycle (Figure S10). Examining the diel variation of POA markers on individual days showed features consistent with the corresponding emission sources or boundary layer height variation, depending on which factor was dominant. For example, decreased daytime concentrations of most species under CL#2&3 were observed, in accordance with the higher boundary layer height in the daytime. The diurnal variations of the POA markers on selected days under each cluster are shown in Figure 5. Description of each group of POA markers and their emission source information will be provided in the following subsections.

BB Emission POA Markers. BB occurs on a large scale in urban, rural, and remote areas and has become a global concern, especially in dry seasons in Southeast Asia, where frequent intense BB activities were observed, leading to local and regional air pollution issues.[36−38] Due to different biomass fuels and burning conditions, the molecular compositions of POA in BB smoke particles are highly variable, and a number of molecular markers are invariably emitted from all BB types. They include three anhydrosugars, i.e., levoglucosan and its two isomers, mannosan and glactosan, and a few specific aromatic acids (e.g., 4-hydroxybenzoic acid).

Levoglucosan and its two less abundant anhydrosugar isomers originate from the pyrolysis of cellulose and hemicelluloses.[39] The concentration of levoglucosan ranged from 1.0−238.4 (45.9 ± 39.2) ng/m^3 during this work. For comparison, levoglucosan previously measured in Shanghai was reported at an average of 161 ng/m^3 in winter in 2011−2012[40] and 339.4 ng/m^3 in 2010.[41] The two isomers mannosan and glactosan correlated well with levoglucosan (R_p: 0.96 and 0.95) and shared similar diurnal patterns (not shown).

The ratio of different markers of the same source can be used to examine the sources and evolution of the OA. The ratio of levoglucosan to its isomers (e.g., mannosan) and K^+ could be used to distinguish different BB types. The levoglucosan to mannosan (L/M) ratio can be applied to distinguish hardwood and softwood burning, while the levoglucosan to K^+ (L/K^+) ratio distinguishes emissions from the burning of crop residuals and wood.[42] The average L/K^+ and L/M ratios in our study were 0.4 ± 0.3 (0.02−3.6) and 34 ± 9 (18−60), respectively. These values fall within the range for crop burning in the ratio−ratio distribution plot that encompasses the major BB types documented in the literature (Figure 6a), suggesting that combustion of crop residuals such as rice straw, wheat straw, and corn straw is a dominant BB source influencing Shanghai. We note that levoglucosan undergoes atmospheric degradation in cloud droplets or in deliquescent particles. Hoffmann et al.[6] estimated that levoglucosan had a half-life time of 3−4 days using laboratory-determined kinetics and a parcel model under simulated winter ambient conditions. If we could correct degradation loss and assume that levoglucosan particles experienced an aging of 3−4 days before reaching our sampling site, the L/K^+ ratio data after correction would shift higher to ∼0.8, still within the regime for crop residue burning in the ratio−ratio plot (Figure 6a).

The diurnal variations of the ratios of the three anhydrosugars (i.e., levoglucosan, mannosan, and glactosan) to K^+ showed higher values in the nighttime, which is opposite to the diurnal variation of O_3 (Figure 6b). There are two possible reasons: (1) BB types differ between daytime and nighttime, for example, more smoldering combustion in the night favoring emissions of anhydrosugars versus more flaming burning in the day favoring more K^+ emission, a diurnal pattern shown in Figure 6b could emerge,[43] and (2) if BB emission types are similar between day and night, the •OH-initiated degradation of the anhydrosugars would lead to lower anhydrosugar to K^+ ratios in the day.[6] Without other corroborating evidence, it is difficult to pin down the driving factor for the observed diurnal pattern.

Lignin is another abundant natural polymer in addition to cellulose and hemicellulose, and it is the most abundant polymeric aromatic organic substance in the plant world. High temperature burning of lignin emits a few specific aromatic acids, which can also serve as unique markers for BB.[44]

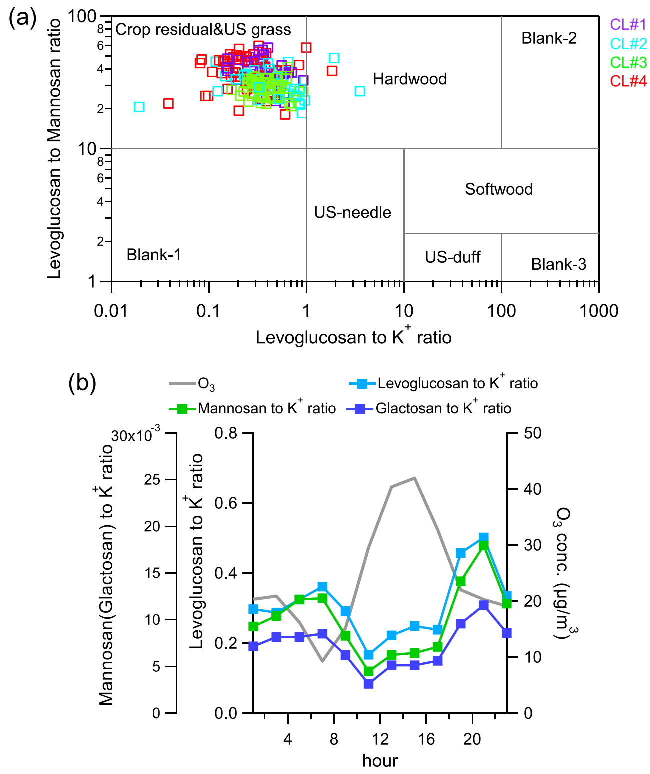

Figure 6. (a) L/K^+ ratios and L/M ratios of the ambient samples collected in Shanghai, with representative ranges of the corresponding ratios for different kinds of biomass obtained from the study by Cheng et al.[42] and (b) diurnal variation of levoglucosan, mannosan, and glactosan to K^+ ratios.

The TAG-measured aromatic acids in this study include 4-hydroxybenzoic acid, 3-hydroxybenzoic acid, terephthalic acid, isophthalic acid, and phthalic acid. Vanillic acid and syringic acid were also detected, but their quantification was compromised by comparable levels present in the blank samples (Text S1.3); therefore, they were not quantified. 4-hydroxybenzoic acid was reported to be related to the burning of lignin (e.g., grass and crop).[45] Although this compound was also reported to be emitted by burning plastics,[46] in our dataset, 4-hydroxybenzoic acid had an excellent correlation with its isomer 3-hydroxybenzoic acid (R_p: 0.95), and the two acids showed excellent correlations with levoglucosan (R_p: 0.87 and 0.86), clearly indicating BB as the dominant source. Among the three phthalic acids, phthalic acid is typically dominated by secondary sources in urban areas and regarded as a SOA tracer derived from the oxidation of naphthalene and its derivatives, while terephthalic and isophthalic acids have more varied and multiple sources.[47,49] Terephthalic acid was reported as a major compound in smoke from burning plastics.[46] However, we note that 1,3,5- triphenylbenzene, which was reported as a marker for plastic burning,[46] was not detected during the entire sampling campaign, negating plastic burning as a significant $PM_{2.5}$ source in urban Shanghai. In this study, isophthalic acid and terephthalic acid are moderately correlated with phthalic acid (R_p: 0.34−0.55), while they show stronger correlations with BC, levoglucosan, and coal combustion tracer As[48] (R_p: 0.63−0.80). These results suggested the significant impact of primary emissions from multiple source origins for the two acids, which limits their utility as unique source markers.

https://dx.doi.org/10.1021/acsearthspacechem.0c00205
ACS Earth Space Chem. 2020, 4, 1670−1685

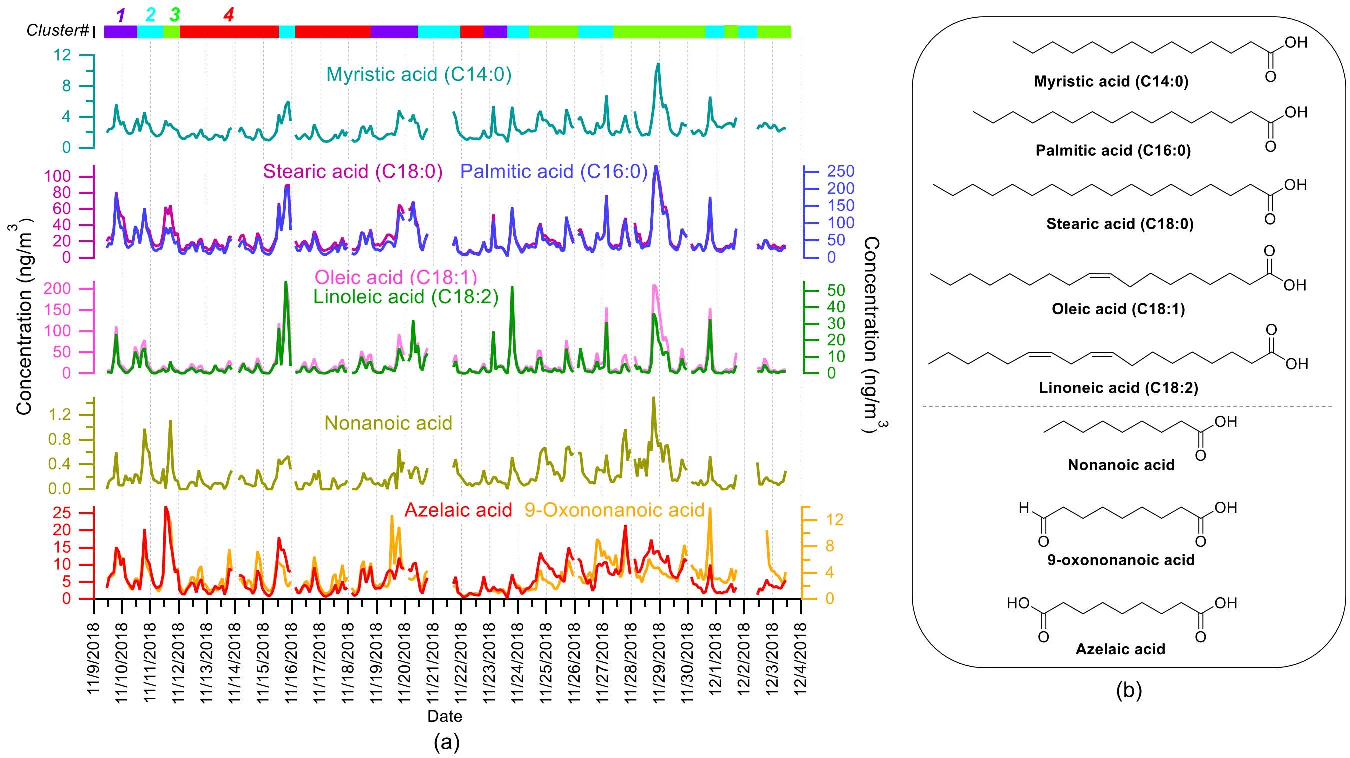

Figure 7. (a) Time series of individual fatty acids related to cooking POA measured in this study and the C_9 acids from oleic acid oxidation, and (b) chemical structures of the corresponding marker species.

Cooking Emission POA Markers. Cooking emission has recently received increasing attention due to its perceived importance in urban environments.[49] It is largely an uncontrolled PM source. The notable contributions of cooking emission to total ambient OA have been addressed in several studies.[50−52] Long straight chain unsaturated and saturated fatty acids (e.g., palmitic acid, stearic acid, and oleic acid), released or formed by hydrolysis and thermal oxidation of cooking oil during the cooking process, are known markers for cooking emissions.[11] C_9 ω-oxo acid and diacids (e.g., 9-oxononanoic acid and azelaic acid) are established in chamber studies as major atmospheric oxidation products from oleic acid ozonolysis,[8−10] and the formation pathways are depicted in Figure S11.

Abundance and Diurnal Variations of Multiple Cooking Emission Markers. The quantified fatty acids in this study include three most abundant saturated fatty acids (myristic acid, palmitic acid, and stearic acid) and two unsaturated fatty acids (oleic acid and linoleic acid). Their chemical structures and concentration time series are shown in Figure 7, together with those of the three C_9 oxidation products. The daily up-and-down was highly synchronous among the five fatty acids, confirming their common sources. On the other hand, the time series of C_9 acids showed different day-to-day variation from those of fatty acids, reflecting different underlying factors driving the diurnal variations.

The total fatty acid concentrations averaged at 105 ng/m^3 and ranged from 7.7 to 629 ng/m^3, comparable to the abundance at an urban site in Hong Kong (92.2 ± 44.1 ng/m^3).[53] The fatty acids showed obvious diurnal variation on most days when zooming into individual days. The dinner time peak was invariably observed under all air mass clusters. The lunch time peak was detected under CL#4 and CL#1, but undetected under CL#2 and CL#3 (Figure 5). Two possible reasons might explain the indistinct lunch time peak: (1) the higher boundary layer height in the daytime facilitated the pollution dispersion and (2) the oxidation of fatty acids after emissions was expected to be stronger during the daytime than the evening. In summary, the distinct dinner time peak of all the fatty acids provides strong evidence for local cooking emissions.

We note that sea spray aerosol is also a source for the fatty acids discussed here. The oleic/stearic acid and palmitic/stearic acid ratios from sea spray aerosol samples are 0.02 and 0.1,[54] which are obviously lower than the ambient data in this study (0.83 ± 0.54 and 1.90 ± 0.37, respectively). Thus, it is reasonable to conclude that sea spray is an insignificant source of fatty acids in urban Shanghai.

Atmospheric Aging of Cooking Markers. Among the five fatty acids, two unsaturated acids (oleic and linoleic) are much more reactive in the atmosphere toward atmospheric oxidants (OH, NO_3, and O_3) as a result of the presence of the C=C bond, in comparison with the three saturated fatty acids. Linoleic acid, with two C=C bonds, is more reactive than oleic acid, which has one C=C bond in its structure. On the other hand, the two saturated fatty acid homologues, palmitic acid and stearic acid, have similar chemical reactivity and volatility, and their ratios should remain mostly unaltered in ambient samples after emissions. Figure 8 plots the oleic/stearic and linoleic/stearic ratios against palmitic/stearic ratios for the measured data in this work. The latter ratio had a narrow range of 0.97−2.85 and an average of 1.90 ± 0.37, slightly lower than the source profile values (2.1−8.1) measured from different restaurants in China.[55−57] The oleic/stearic ratios were 0.83 ± 0.54 (0.12−2.78), also lower than the source profile values (1.2−6.5),[55−57] while linoleic/stearic ratios were 0.14 ± 0.12 (0.01−0.88), approximately one order of magnitude lower than those from source profiles

https://dx.doi.org/10.1021/acsearthspacechem.0c00205
ACS Earth Space Chem. 2020, 4, 1670−1685

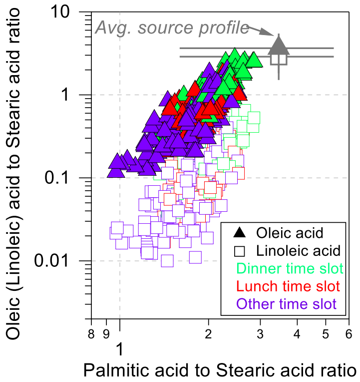

Figure 8. Oleic acid and linoleic acid to stearic acid ratios versus palmitic acid to stearic acid ratio of the ambient samples collected in Shanghai. The averaged ratios from different cooking emission profiles obtained from previous studies[55−57] are also shown in the plot. The ambient data are color coded by the dinner time slot (17:00−21:00, green), lunch time slot (09:00−13:00, red), and other time slot (purple).

(1.1−5.8),[55−57] clearly indicating degradation after emissions. The oleic/stearic ratio was comparable to those measured in winter in Beijing (0.65).[58] The spread in the oleic/stearic (0.12−2.78) and linoleic/stearic (0.01−0.88) ratios is noticeably larger than that of the palmitic/stearic ratios (0.97−2.85), also confirming that the two unsaturated acids are more susceptible to atmospheric degradation. In addition, the individual linoleic/stearic ratios were consistently lower than the oleic/stearic ratios (Figure 8), reflecting the higher reactivity of linoleic acid than oleic acid.

Figure 8 also allows us to examine the ratio data segregated by mealtimes and nonmeal times by color-coding lunch time, dinner time, and other time slots. The ratios are obviously higher during dinner (17:00−21:00) and lunch time (09:00−13:00) as a result of more fresh emissions introduced into the ambient atmosphere, again further supporting that local cooking emissions influence the sampling site.

The ozone attack of oleic acid leads to the formation of C_9 aldehyde and acids, i.e., nonanal, azelaic acid, nonanoic acid, and 9-oxononanoic acid,[8−10] among which nonanal is mainly in the gas phase and was therefore unmeasured by TAG. Azelaic acid was positively identified in the chromatograms of our ambient samples using authentic standards, while nonanoic acid was tentatively identified by excellent match with its mass spectrum in the NIST library. Identification of 9-oxononanoic acid was based on comparison of its mass spectrum with that reported by Pleik et al.[59] (details provided in Text S2). Among the three identified products, azelaic acid has the lowest volatility. Thus, its particle-phase presence was least influenced by gas-particle re-partitioning, and for this reason, we examine in detail this compound in the following analysis.

Figure 9a shows correlations between azelaic acid and oleic acid, both normalized by stearic acid, with data segregated into two groups by air mass clusters. Under the influence of local/median-range air masses (CL#2&3), azelaic acid was negatively correlated with oleic acid (Figure 9a, left panel). A representative diurnal variation on a CL#3-influenced day

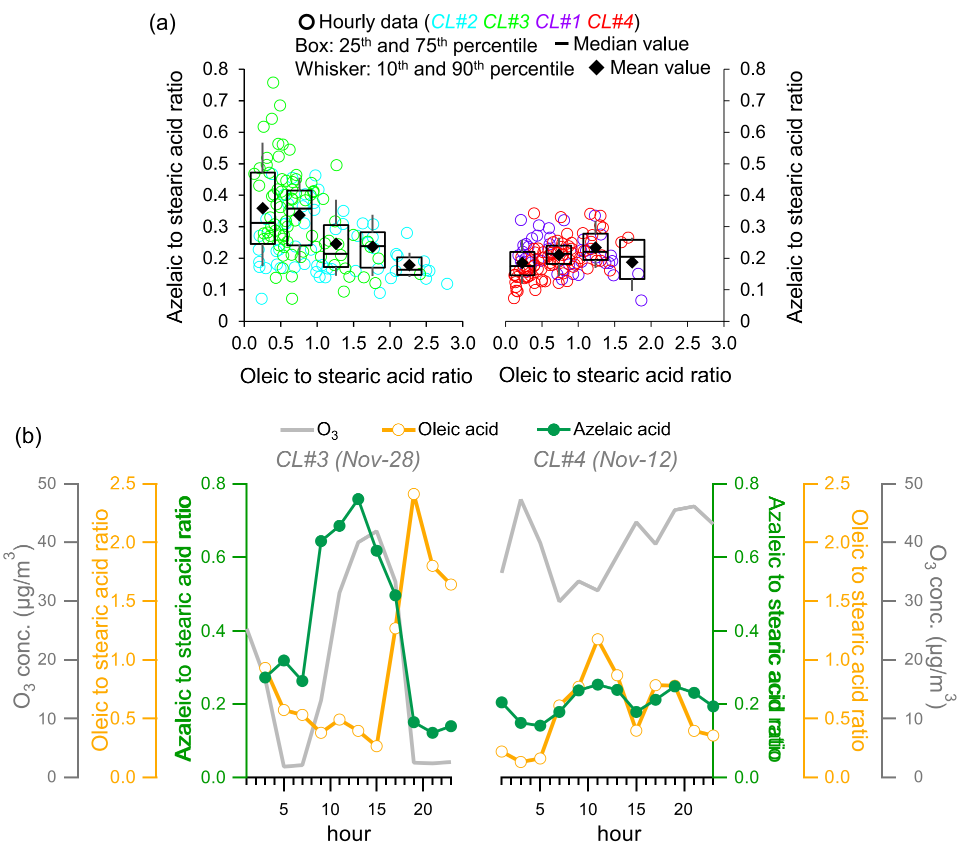

Figure 9. (a) Correlation of azelaic acid with oleic acid normalized by stearic acid for the ambient samples, separated by local/median-range transport air mass (CL#2&3) and long-range transport air mass (CL#1&4). (b) Diurnal variation of azelaic acid and oleic acid normalized by stearic acid and O_3 concentrations for selected individual days (28 Nov., CL#3 and 12 Nov., CL#4).

https://dx.doi.org/10.1021/acsearthspacechem.0c00205
ACS Earth Space Chem. 2020, 4, 1670−1685

(28 Nov.) (Figure 9b, left panel) shows a clear ozone peak in early afternoon, characteristic of local ozone formation. Additionally, the diel variation trend of azelaic acid roughly tracked that of ozone, while it was opposite to that of oleic acid. Around noontime, azelaic acid peaked, while oleic acid was most depleted, in line with their known product–precursor relationship in the oleic acid ozonolysis reaction. Under long range transport influence (CL#1&4), which was associated with higher O_3 concentrations, the correlation between azelaic acid and oleic acid was clearly dissimilar to that under the influence of CL#2&3, and a negative correlation was absent (Figure 9a, right panel). Taking 12 Nov. as an example of a CL#4-influenced day, we note it had a few clear differences in comparison with 28 Nov., the CL#3-influenced day. Specifically, azelaic acid varied in sync with oleic acid, and both had an opposite variation pattern to that of O_3 (Figure 9b, right panel), the level of which was significantly higher than that observed on 28 Nov. These observations were consistent with more aged aerosol from long range transportation. A similar plot to Figure 9, but including all three C_9 products, is shown in Figure S15. The diurnal behaviors of 9-oxononanoic acid were similar to those of azelaic acid under all air mass cluster types, further supporting oleic acid ozonolysis as the major degradation pathway in this urban environment. As for nonanoic acid, its concentrations in the particle-phase were much lower due to its high volatility, and only a small fraction of total nonanoic acid was captured as a PM component by TAG. Thus, its relationship with oleic acid was not as clear as the other two C_9 products.

The oleic/stearic ratio indicates the aging of cooking aerosols,[60] while the O/C ratio measured by AMS reflects the degree of oxygenation of OA. The scatter plot of these two ratios (Figure 10) shows a moderate negative correlation (R_p: −0.66). This result is inspiring as the oleic/stearic ratio is linked to the specific oxidation processing of oleic acid in the atmosphere. The oleic acid–ozone heterogeneous reaction has been widely studied as a model heterogeneous reaction system to represent the oxidative processing of OA.[9] The observed correlation implies that the heterogeneous reaction of particle phase unsaturated species such as oleic acid may represent a significant oxidation process of total OA in urban areas.

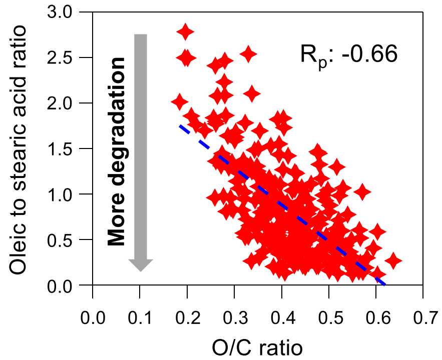

Figure 10. Correlation of the oleic/stearic ratio from TAG measurements with the O/C ratio from AMS.

PAHs and Their Sources. PAHs are formed during the incomplete combustion of any carbonaceous materials, the common ones including fossil fuels, biomass, garbage, and coal.[61] The relative contributions from different sources are geographically and seasonally dependent. Automobile exhaust was recognized as one of the main PAH contributors in outdoor environments in Mexico city.[62] Coal combustion and BB were also found as important contributors for PAHs in Chinese cities, especially in winter.[63,64] Lee and Kim[65] also reported significant contribution of long range transport of PAHs from Northeast Asia in urban Seoul especially in Winter.

The PAHs quantified in this study include fluoranthene, pyrene, chrysene, benz[a]anthracene (BaA), benzo[b]-fluoranthene (BbF), benzo[k]fluoranthene (BkF), benzo[e]-pyrene (BeP), benzo[a]pyrene (BaP), perylene, benzo[ghi]-perylene (BghiP), and indeno[1,2,3-cd]pyrene (IcdP). Concentrations of the total quantified PAHs ranged from 0.38–21.2 (3.54 ± 3.16) ng/m^3. The measured PAH levels were comparable to previous studies in Shanghai.[66,67] Diurnal variations of BghiP and BeP on select individual days representing the four air mass clusters are shown as examples in Figure 5. Obvious morning and afternoon peaks around traffic rush hours were observed for most days especially under CL#3, in sync with the variation of NO_x, indicating a strong impact from local traffic emissions, whereas under CL#4, no diurnal variation of PAHs was observed. Elorduy et al.[16] observed the highest PM_{10} PAH level in the afternoon and night hours (20:00–04:00) in northern Spain in Nov. and Dec. 2013, while Gu et al.[19] observed the highest PAH level in the morning (06:30–10:00) in 18–19 Dec. 2006 in urban Shanghai. BghiP showed much higher concentrations under CL#1 and CL#3 and the lowest concentrations under CL#4. It correlated well with other measured PAH homologues (R_p: 0.81–0.97).

We examined the ratio–ratio plot of two pairs of PAH homologues (i.e., BaP vs BeP and BghiP vs IcdP) normalized against BC to inform the dominant sources of PAH species (Figure 11). Under CL#1&4, ambient data are closer to the source profiles of coal combustion and BB, suggesting more influence from these two combustion sources, whereas under CL#2&3, ambient data are distributed toward the lower left corner, closer to the tunnel emission profiles, indicating more influence from local vehicle emissions. The measured PAH species showed good correlations with levoglucosan (R_p: 0.76) and moderate correlations with BC and As. Correlations of PAHs with the major combustion source tracers separated by different clusters are plotted in Figure S16. Good correlations with As and BC under CL#1 were observed, with the slope much higher than other clusters, indicating additional regional source input of the PAHs from the northern continental area. Under CL#3, with enhanced impact from local emissions, PAHs showed good correlations with BC when excluding some outliers, consistent with the vehicle emission input for PAHs under local air mass influence. However, the lack of source-specific tracers for vehicle emissions (such as hopanes[56]) limits our ability in ascertaining the association of PAHs to the vehicular source.

Source Analysis Using Positive Matrix Factorization. To gain a more quantitative assessment of source contributions of the abovementioned source categories to OA, we carried out receptor modeling using positive matrix factorization (PMF).[76] The target POA markers were incorporated into the input data matrix, along with SOA markers (Table S2) and major aerosol components including major ions, elements, EC, and OC. At our monitoring site (SAES), OC and EC were not available; we thereby “borrowed” the OC and EC data from a nearby urban monitoring station, which was 12 km away (site name: Pudong). We note that a detailed source apportionment

https://dx.doi.org/10.1021/acsearthspacechem.0c00205
ACS Earth Space Chem. 2020, 4, 1670−1685

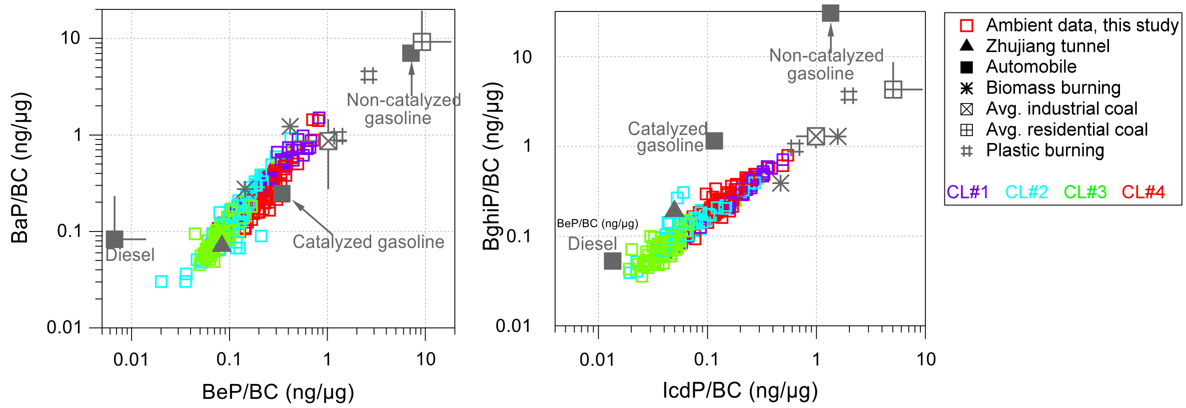

Figure 11. Ratio−ratio plot of BaP and BeP normalized by BC (left) and BghiP and IcdP normalized by BC (right) for the ambient samples collected in Shanghai, color-coded by cluster numbers. The ratio for the Zhujiang tunnel profile is from He et al.,[68] and automobile emission profiles are averaged from a number of published profiles.[69−72] Residential and industrial coal combustion source profiles are from Zhang et al.[73] The BB source profile is from Yu.[74] The plastic burning source profile is from Gu et al.[75]

analysis utilizing the same set of organic source markers measured in this field campaign is reported in a separate paper by Li et al.,[29] in combination with inorganic ions and elemental species at Pudong.[29] Between the SAES site in this work and the Pudong site, their $PM_{2.5}$ levels were in excellent agreement and highly in sync, as seen in their nearly overlapping time series, and a slope of 0.95 and a correlation coefficient of 0.96 in their scatter correlation plot (Figure S17). Such a high degree of similarity in $PM_{2.5}$ indicates that the two sites are influenced by the same PM pollution sources. Expectedly, PMF results in this work are essentially similar to those obtained by Li et al.[29] We refer readers to the study by Li et al.[29] for details of the PMF modeling and discussion of source apportionment results. Below we will only present PMF results related to the abovementioned POA markers. Identification of each PMF-resolved source factor is shown in Text S3.

Briefly, an 11-factor solution was determined to be the most optimal as it gives the most reasonable source profiles and at the same time meets various diagnostic criteria of the PMF modeling. The resolved sources are the secondary nitrate formation process, secondary sulfate formation process, SOA factor, vehicle exhaust, industrial emission/tire wear, industrial emission, residual oil combustion, coal combustion, dust, BB, and cooking. Among them, three factors that are dominated by OA, namely the SOA factor, BB, and cooking emissions, were only resolved by PMF due to the incorporation of the unique organic tracer data in PMF.[29] The resolved factor profiles and time series of factor contributions to OC are shown in Figure S18. The average source contributions to OC from the PMF results are shown in Figure 12 and those to $PM_{2.5}$ are shown in Figure S19. The cooking emission factor profile was characterized by high loadings of saturated fatty acids and C_9 acids, and this factor contributed to 14.5% of total OC. Vehicle exhaust, resolved by high loadings of EC, was another important source to OC, contributing to 18.5%. BB, identified by high loadings of levoglucosan and mannosan, contributed to 1.9% of total OC. It should be noted that phthalic acid was mainly attributed to secondary source factors (secondary nitrate, secondary sulfate, and SOA factor), while isophthalic acid and terephthalic acid were distributed among multiple source factors including both POA and SOA. Majority of the PAHs were attributed to the BB factor and were driven by the high concentrations under long-range transport air mass. In summary, there is a good consistency between the quantitative

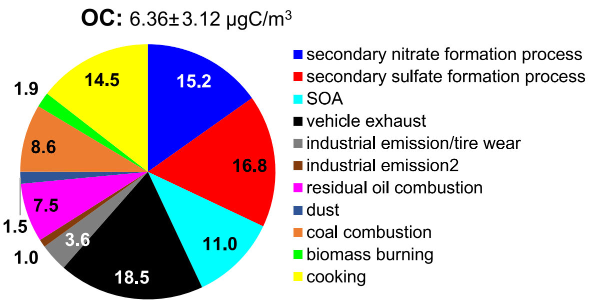

Figure 12. Percentage contributions of individual source factors to OC.

source assessment by PMF and the qualitative source characterization discussed earlier.

Implications of Hourly POA Marker Data. This work demonstrates that hourly measurements of organic markers are effective in providing more detailed chemical information to capture the dynamic changes of the source contributions and their chemical evolution. The unique source-specific features of the organic molecular markers coupled with the hourly observed variability can improve our ability to use receptor modeling (such as PMF) to resolve and subsequently estimate contributions of the multiple sources that would otherwise remain unseparated. When TAG is operated side-by-side with AMS, the molecular marker data by TAG could also be valuable in facilitating resolving bulk OA measured by AMS into more specific source types. Such measurements of hourly molecular markers at multiple sites are suggested in the future to allow examination of spatial variation characteristics and cross-comparison of source identification so that more accurate source apportionment can be achieved.

The online TAG measurements also enable field observations of chemical evolution of a specific primary OA source through tracking the relative abundance of molecular markers of different reactivities from this source (e.g., unsaturated and saturated fatty acids from cooking). Such a high level of molecular specificity is not possible with the currently more widely deployed instruments, such as AMS, which measure bulk OA. The field monitoring of paired molecular markers may provide an opportunity to link observations made in chamber or laboratory studies with those in the real

https://dx.doi.org/10.1021/acsearthspacechem.0c00205
ACS Earth Space Chem. 2020, 4, 1670−1685

atmosphere, thereby informing the parameterization of OA aging in numerical modeling of air quality and climate.

ASSOCIATED CONTENT

Supporting Information

The Supporting Information is available free of charge at https://pubs.acs.org/doi/10.1021/acsearthspacechem.0c00205.

Schematic figure of the TAG system, data validation of TAG and other measurements, temporal variation of gas pollutants and meteorological parameters, identification of C_9 acids in ambient samples, source evaluation of PAHs under different clusters, PMF source profiles and contributions (PDF).

AUTHOR INFORMATION

Corresponding Authors

Cheng Huang − *State Environmental Protection Key Laboratory of the Formation and Prevention of Urban Air Pollution Complex, Shanghai Academy of Environmental Sciences, Shanghai 200233, China;* orcid.org/0000-0001-9518-3628; Email: huangc@saes.sh.cn

Jian Zhen Yu − *Department of Chemistry and Division of Environment & Sustainability, The Hong Kong University of Science & Technology, Hong Kong, China;* orcid.org/0000-0002-6165-6500; Email: jian.yu@ust.hk

Authors

Qiongqiong Wang − *Department of Chemistry, The Hong Kong University of Science & Technology, Hong Kong, China*

Xiao He − *Division of Environment & Sustainability, The Hong Kong University of Science & Technology, Hong Kong, China*

Min Zhou − *State Environmental Protection Key Laboratory of the Formation and Prevention of Urban Air Pollution Complex, Shanghai Academy of Environmental Sciences, Shanghai 200233, China*

Dan Dan Huang − *State Environmental Protection Key Laboratory of the Formation and Prevention of Urban Air Pollution Complex, Shanghai Academy of Environmental Sciences, Shanghai 200233, China;* orcid.org/0000-0003-2878-7469

Liping Qiao − *State Environmental Protection Key Laboratory of the Formation and Prevention of Urban Air Pollution Complex, Shanghai Academy of Environmental Sciences, Shanghai 200233, China*

Shuhui Zhu − *Division of Environment & Sustainability, The Hong Kong University of Science & Technology, Hong Kong, China; State Environmental Protection Key Laboratory of the Formation and Prevention of Urban Air Pollution Complex, Shanghai Academy of Environmental Sciences, Shanghai 200233, China*

Ying-ge Ma − *State Environmental Protection Key Laboratory of the Formation and Prevention of Urban Air Pollution Complex, Shanghai Academy of Environmental Sciences, Shanghai 200233, China*

Hong-li Wang − *State Environmental Protection Key Laboratory of the Formation and Prevention of Urban Air Pollution Complex, Shanghai Academy of Environmental Sciences, Shanghai 200233, China;* orcid.org/0000-0003-0655-3389

Li Li − *Institute of Environmental Pollution and Health, Shanghai University, Shanghai 200072, China*

X. H. Hilda Huang − *Division of Environment & Sustainability, The Hong Kong University of Science & Technology, Hong Kong, China;* orcid.org/0000-0001-6381-3242

Wen Xu − *Aerodyne Research Inc., Billerica, Massachusetts 01821, United States*

Douglas Worsnop − *Aerodyne Research Inc., Billerica, Massachusetts 01821, United States*

Allen H. Goldstein − *Department of Environmental Science, Policy, and Management and Department of Civil and Environmental Engineering, University of California, Berkeley, California 94720, United States;* orcid.org/0000-0003-4014-4896

Hai Guo − *Department of Civil and Environmental Engineering, The Hong Kong Polytechnic University, Hong Kong, China;* orcid.org/0000-0002-7996-7294

Complete contact information is available at: https://pubs.acs.org/10.1021/acsearthspacechem.0c00205

Notes

The authors declare no competing financial interest.

ACKNOWLEDGMENTS

We are thankful for funding support from the National Key R&D Program of China (2018YFC0213800), the National Natural Science Foundation of China (41875161), the Hong Kong Research Grants Council (C5004-15E, 16305418, and R6011-18), and the Hong Kong University of Science & Technology (VPRDO19IP01).

REFERENCES

(1) Kanakidou, M.; Seinfeld, J. H.; Pandis, S. N.; Barnes, I.; Dentener, F. J.; Facchini, M. C.; Van Dingenen, R.; Ervens, B.; Nenes, A.; Nielsen, C. J.; Swietlicki, E.; Putaud, J.-P.; Balkanski, Y.; Sandro, F.; Horth, J.; Moortgat, G.; Winterhalter, R.; Lund Myhre, C.; Tsigaridis, K.; Wilson, J. Organic Aerosol and Global Climate Modelling: A Review. *Atmos. Chem. Phys.* **2005**, *5*, 1053−1123.

(2) Hamilton, J. F.; Webb, P. J.; Lewis, A. C.; Hopkins, J. R.; Smith, S.; Davy, P. Partially Oxidised Organic Components in Urban Aerosol Using GCXGC-TOF/MS. *Atmos. Chem. Phys.* **2004**, *4*, 1279−1290.

(3) Jaeckels, J. M.; Bae, M. S.; Schauer, J. J. Positive Matrix Factorization (PMF) Analysis of Molecular Marker Measurements to Quantify the Sources of Organic Aerosols. *Environ. Sci. Technol.* **2007**, *41*, 5763−5769.

(4) Shrivastava, M. K.; Subramanian, R.; Rogge, W. F.; Robinson, A. L. Sources of Organic Aerosol: Positive Matrix Factorization of Molecular Marker Data and Comparison of Results from Different Source Apportionment Models. *Atmos. Environ.* **2007**, *41*, 9353−9369.

(5) Wang, Q.; He, X.; Hilda Huang, X. H.; Griffith, S. M.; Feng, Y.; Zhang, T.; Zhang, Q.; Wu, D.; Yu, J. Z. Impact of Secondary Organic Aerosol Tracers on Tracer-Based Source Apportionment of Organic Carbon and Pm 2.5 : A Case Study in the Pearl River Delta, China. *ACS Earth Space Chem.* **2017**, *1*, 562−571.

(6) Hoffmann, D.; Tilgner, A.; Iinuma, Y.; Herrmann, H. Atmospheric Stability of Levoglucosan: A Detailed Laboratory and Modeling Study. *Environ. Sci. Technol.* **2010**, *44*, 694−699.

(7) Ringuet, J.; Leoz-Garziandia, E.; Budzinski, H.; Villenave, E.; Albinet, A. Particle Size Distribution of Nitrated and Oxygenated Polycyclic Aromatic Hydrocarbons (NPAHs and OPAHs) on Traffic and Suburban Sites of a European Megacity: Paris (France). *Atmos. Chem. Phys.* **2012**, *12*, 8877−8887.

(8) Vesna, O.; Sax, M.; Kalberer, M.; Gaschen, A.; Ammann, M. Product Study of Oleic Acid Ozonolysis as Function of Humidity. *Atmos. Environ.* **2009**, *43*, 3662−3669.

(9) Zahardis, J.; Petrucci, G. A. The Oleic Acid-Ozone Heterogeneous Reaction System : Products , Kinetics, Secondary Chemistry, and Atmospheric Implications of a Model System − a Review. *Atmos. Chem. Phys.* **2007**, *7*, 1237−1274.
(10) Ziemann, P. J. Aerosol Products, Mechanisms, and Kinetics of Heterogeneous Reactions of Ozone with Oleic Acid in Pure and Mixed Particles. *Faraday Discuss.* **2005**, *130*, 469−490.
(11) Rogge, W. F.; Hildemann, L. M.; Mazurek, M. A.; Cass, G. R.; Simoneit, B. R. T. Sources of Fine Organic Aerosol. 1. Charbroilers and Meat Cooking Operations. *Environ. Sci. Technol.* **1991**, *25*, 1112−1125.
(12) DeCarlo, P. F.; Kimmel, J. R.; Trimborn, A.; Northway, M. J.; Jayne, J. T.; Aiken, A. C.; Gonin, M.; Fuhrer, K.; Horvath, T.; Docherty, K. S.; et al. Field-Deployable, High-Resolution, Time-of-Flight Aerosol Mass Spectrometer. *Anal. Chem.* **2006**, *78*, 8281−8289.
(13) Dall'Osto, M.; Harrison, R. M. Urban Organic Aerosols Measured by Single Particle Mass Spectrometry in the Megacity of London. *Atmos. Chem. Phys.* **2012**, *12*, 4127−4142.
(14) Sullivan, R. C.; Prather, K. A. Recent Advances in Our Understanding of Atmospheric Chemistry and Climate Made Possible by On-Line Aerosol Analysis Instrumentation. *Anal. Chem.* **2005**, *77*, 3861−3886.
(15) Chen, D.; Bi, X.; Zhao, J.; Chen, L.; Tan, J.; Mai, B.; Sheng, G.; Fu, J.; Wong, M. Pollution Characterization and Diurnal Variation of PBDEs in the Atmosphere of an E-Waste Dismantling Region. *Environ. Pollut.* **2009**, *157*, 1051−1057.
(16) Elorduy, I.; Elcoroaristizabal, S.; Durana, N.; García, J. A.; Alonso, L. Diurnal Variation of Particle-Bound PAHs in an Urban Area of Spain Using TD-GC/MS: Influence of Meteorological Parameters and Emission Sources. *Atmos. Environ.* **2016**, *138*, 87−98.
(17) Fu, P.; Kawamura, K. Diurnal Variations of Polar Organic Tracers in Summer Forest Aerosols: A Case Study of a Quercus and Picea Mixed Forest in Hokkaido, Japan. *Geochem. J.* **2011**, *45*, 297−308.
(18) Fu, P. Q.; Kawamura, K.; Chen, J.; Li, J.; Sun, Y. L.; Liu, Y.; Tachibana, E.; Aggarwal, S. G.; Okuzawa, K.; Tanimoto, H.; et al. Diurnal Variations of Organic Molecular Tracers and Stable Carbon Isotopic Composition in Atmospheric Aerosols over Mt. Tai in the North China Plain: An Influence of Biomass Burning. *Atmos. Chem. Phys.* **2012**, *12*, 8359−8375.
(19) Gu, Z.; Feng, J.; Han, W.; Li, L.; Wu, M.; Fu, J.; Sheng, G. Diurnal Variations of Polycyclic Aromatic Hydrocarbons Associated with PM 2.5 in Shanghai, China. *J. Environ. Sci.* **2010**, *22*, 389−396.
(20) Liu, J.; Li, J.; Lin, T.; Liu, D.; Xu, Y.; Chaemfa, C.; Qi, S.; Liu, F.; Zhang, G. Diurnal and Nocturnal Variations of PAHs in the Lhasa Atmosphere, Tibetan Plateau: Implication for Local Sources and the Impact of Atmospheric Degradation Processing. *Atmos. Res.* **2013**, *124*, 34−43.
(21) Wei, S.; Huang, B.; Liu, M.; Bi, X.; Ren, Z.; Sheng, G.; Fu, J. Characterization of PM2.5-Bound Nitrated and Oxygenated PAHs in Two Industrial Sites of South China. *Atmos. Res.* **2012**, *109-110*, 76−83.
(22) Ma, Y.; Xu, X.; Song, W.; Geng, F.; Wang, L. Seasonal and Diurnal Variations of Particulate Organosulfates in Urban Shanghai, China. *Atmos. Environ.* **2014**, *85*, 152−160.
(23) Williams, B. J.; Goldstein, A. H.; Kreisberg, N. M.; Hering, S. V. An In-Situ Instrument for Speciated Organic Composition of Atmospheric Aerosols: Thermal Desorption Aerosol GC/MS-FID (TAG). *Aerosol Sci. Technol.* **2006**, *40*, 627−638.
(24) Kreisberg, N. M.; Worton, D. R.; Zhao, Y.; Isaacman, G.; Goldstein, A. H.; Hering, S. V. Development of an Automated High-Temperature Valveless Injection System for Online Gas Chromatography. *Atmos. Meas. Tech.* **2014**, *7*, 4431−4444.
(25) Lambe, A. T.; Logue, J. M.; Kreisberg, N. M.; Hering, S. V.; Worton, D. R.; Goldstein, A. H.; Donahue, N. M.; Robinson, A. L. Apportioning Black Carbon to Sources Using Highly Time-Resolved Ambient Measurements of Organic Molecular Markers in Pittsburgh. *Atmos. Environ.* **2009**, *43*, 3941−3950.
(26) Isaacman, G.; Kreisberg, N. M.; Yee, L. D.; Worton, D. R.; Chan, A. W. H.; Moss, J. A.; Hering, S. V.; Goldstein, A. H. Online Derivatization for Hourly Measurements of Gas- and Particle-Phase Semi-Volatile Oxygenated Organic Compounds by Thermal Desorption Aerosol Gas Chromatography (SV-TAG). *Atmos. Meas. Tech.* **2014**, *7*, 4417−4429.
(27) Williams, B. J.; Goldstein, A. H.; Kreisberg, N. M.; Hering, S. V.; Worsnop, D. R.; Ulbrich, I. M.; Docherty, K. S.; Jimenez, J. L. Major Components of Atmospheric Organic Aerosol in Southern California as Determined by Hourly Measurements of Source Marker Compounds. *Atmos. Chem. Phys.* **2010**, *10*, 11577−11603.
(28) Zhao, Y.; Kreisberg, N. M.; Worton, D. R.; Isaacman, G.; Gentner, D. R.; Chan, A. W. H.; Weber, R. J.; Liu, S.; Day, D. A.; Russell, L. M.; Hering, S. V.; Goldstein, A. H. Sources of Organic Aerosol Investigated Using Organic Compounds as Tracers Measured during CalNex in Bakersfield. *J. Geophys. Res. Atmos.* **2013**, *118*, 11388−11,398.
(29) Li, R.; Wang, Q.; He, X.; Zhu, S.; Zhang, K.; Duan, Y.; Fu, Q.; Qiao, L.; Wang, Y.; Huang, L.; Li, L.; Yu, J. Source Apportionment of PM2.5 in Shanghai Based on Hourly Molecular Organic Markers and Other Source Tracers. *Atmos. Chem. Phys. Discuss.* **2020**, 1−26.
(30) He, X.; Wang, Q.; Huang, X. H.; Huang, D. D.; Zhou, M.; Qiao, L.; Zhu, S.; Ma, Y.-G.; Wang, H.-L.; Li, L.; Huang, C.; Xu, W.; Worsnop, D. R.; Goldsten, A. H.; Yu, J. Z. Hourly Measurements of Organic Molecular Markers in Urban Shanghai, China: Observation of Enhanced Formation of Secondary Organic Aerosol during Particulate Matter Episodic Periods. *Atmos. Environ.* **2020**, 117807.
(31) Wang, Q.; Qiao, L.; Zhou, M.; Zhu, S.; Griffith, S.; Li, L.; Yu, J. Z. Source Apportionment of PM 2.5 Using Hourly Measurements of Elemental Tracers and Major Constituents in an Urban Environment: Investigation of Time-Resolution Influence. *J. Geophys. Res. Atmos.* **2018**, *123*, 5284−5300.
(32) Zhao, Y.; Kreisberg, N. M.; Worton, D. R.; Teng, A. P.; Hering, S. V.; Goldstein, A. H. Development of an in Situ Thermal Desorption Gas Chromatography Instrument for Quantifying Atmospheric Semi-Volatile Organic Compounds. *Aerosol Sci. Technol.* **2013**, *47*, 258−266.
(33) Isaacman-VanWertz, G.; Sueper, D. T.; Aikin, K. C.; Lerner, B. M.; Gilman, J. B.; de Gouw, J. A.; Worsnop, D. R.; Goldstein, A. H. Automated Single-Ion Peak Fitting as an Efficient Approach for Analyzing Complex Chromatographic Data. *J. Chromatogr. A* **2017**, *1529*, 81−92.
(34) Qiao, L.; Cai, J.; Wang, H.; Wang, W.; Zhou, M.; Lou, S.; Chen, R.; Dai, H.; Chen, C.; Kan, H. PM2.5 Constituents and Hospital Emergency-Room Visits in Shanghai, China. *Environ. Sci. Technol.* **2014**, *48*, 10406−10414.
(35) Lin, W.; Xu, X.; Ma, Z.; Zhao, H.; Liu, X.; Wang, Y. Characteristics and Recent Trends of Sulfur Dioxide at Urban, Rural, and Background Sites in North China: Effectiveness of Control Measures. *J. Environ. Sci.* **2012**, *24*, 34−49.
(36) Engling, G.; He, J.; Betha, R.; Balasubramanian, R. Assessing the Regional Impact of Indonesian Biomass Burning Emissions Based on Organic Molecular Tracers and Chemical Mass Balance Modeling. *Atmos. Chem. Phys.* **2014**, *14*, 8043−8054.
(37) Budisulistiorini, S. H.; Riva, M.; Williams, M.; Miyakawa, T.; Chen, J.; Itoh, M.; Surratt, J. D.; Kuwata, M. Dominant Contribution of Oxygenated Organic Aerosol to Haze Particles from Real-Time Observation in Singapore during an Indonesian Wildfire Event in 2015. *Atmos. Chem. Phys.* **2018**, *18*, 16481−16498.
(38) Fujii, Y.; Tohno, S.; Amil, N.; Latif, M. T. Quantitative Assessment of Source Contributions to PM2.5 on the West Coast of Peninsular Malaysia to Determine the Burden of Indonesian Peatland Fire. *Atmos. Environ.* **2017**, *171*, 111−117.
(39) Simoneit, B. R. T. Biomass Burning - A Review of Organic Tracers for Smoke from Incomplete Combustion. *Appl. Geochem.* **2002**, *17*, 129−162.
(40) Li, X.; Chen, M.; Le, H. P.; Wang, F.; Guo, Z.; Iinuma, Y.; Chen, J.; Herrmann, H. Atmospheric Outflow of PM2.5 Saccharides

from Megacity Shanghai to East China Sea: Impact of Biological and Biomass Burning Sources. *Atmos. Environ.* **2016**, *143*, 1−14.

(41) Feng, J.; Li, M.; Zhang, P.; Gong, S.; Zhong, M.; Wu, M.; Zheng, M.; Chen, C.; Wang, H.; Lou, S. Investigation of the Sources and Seasonal Variations of Secondary Organic Aerosols in PM2.5 in Shanghai with Organic Tracers. *Atmos. Environ.* **2013**, *79*, 614−622.

(42) Cheng, Y.; Engling, G.; He, K. B.; Duan, F. K.; Ma, Y. L.; Du, Z. Y.; Liu, J. M.; Zheng, M.; Weber, R. J. Biomass Burning Contribution to Beijing Aerosol. *Atmos. Chem. Phys.* **2013**, *13*, 7765−7781.

(43) Schkolnik, G.; Falkovich, A. H.; Rudich, Y.; Maenhaut, W.; Artaxo, P. New Analytical Method for the Determination of Levoglucosan, Polyhydroxy Compounds, and 2-Methylerythritol and Its Application to Smoke and Rainwater Samples. *Environ. Sci. Technol.* **2005**, *39*, 2744−2752.

(44) Wan, X.; Kawamura, K.; Ram, K.; Kang, S.; Loewen, M.; Gao, S.; Wu, G.; Fu, P.; Zhang, Y.; Bhattarai, H.; Cong, Z. Aromatic Acids as Biomass-Burning Tracers in Atmospheric Aerosols and Ice Cores : A Review. *Environ. Pollut.* **2019**, *247*, 216−228.

(45) Wan, X.; Kang, S.; Li, Q.; Rupakheti, D.; Zhang, Q.; Guo, J.; Chen, P.; Tripathee, L.; Rupakheti, M.; Panday, A. K.; Wang, W.; Kawamura, K.; Gao, S.; Wu, G.; Cong, Z. Organic Molecular Tracers in the Atmospheric Aerosols from Lumbini, Nepal, in the Northern Indo-Gangetic Plain : Influence of Biomass Burning. *Atmos. Chem. Phys.* **2017**, *17*, 8867−8885.

(46) Simoneit, B. R. T.; Medeiros, P. M.; Didyk, B. M. Combustion Products of Plastics as Indicators for Refuse Burning in the Atmosphere. *Environ. Sci. Technol.* **2005**, *39*, 6961−6970.

(47) Kleindienst, T. E.; Jaoui, M.; Lewandowski, M.; Offenberg, J. H.; Docherty, K. S. The Formation of SOA and Chemical Tracer Compounds from the Photooxidation of Naphthalene and Its Methyl Analogs in the Presence and Absence of Nitrogen Oxides. *Atmos. Chem. Phys.* **2012**, *12*, 8711−8726.

(48) Chen, J.; Liu, G.; Kang, Y.; Wu, B.; Sun, R.; Zhou, C.; Wu, D. Atmospheric Emissions of F, As, Se, Hg, and Sb from Coal-Fired Power and Heat Generation in China. *Chemosphere* **2013**, *90*, 1925−1932.

(49) Abdullahi, K. L.; Delgado-Saborit, J. M.; Harrison, R. M. Emissions and Indoor Concentrations of Particulate Matter and Its Specific Chemical Components from Cooking: A Review. *Atmos. Environ.* **2013**, *71*, 260−294.

(50) Huang, X. F.; He, L. Y.; Hu, M.; Canagaratna, M. R.; Sun, Y.; Zhang, Q.; Zhu, T.; Xue, L.; Zeng, L. W.; Liu, X. G.; et al. Highly Time-Resolved Chemical Characterization of Atmospheric Submicron Particles during 2008 Beijing Olympic Games Using an Aerodyne High-Resolution Aerosol Mass Spectrometer. *Atmos. Chem. Phys.* **2010**, *10*, 8933−8945.

(51) Sun, Y. L.; Wang, Z. F.; Fu, P. Q.; Yang, T.; Jiang, Q.; Dong, H. B.; Li, J.; Jia, J. J. Aerosol Composition, Sources and Processes during Wintertime in Beijing, China. *Atmos. Chem. Phys.* **2013**, *13*, 4577−4592.

(52) Sun, C.; Lee, B. P.; Huang, D.; Jie Li, Y.; Schurman, M. I.; Louie, P. K. K.; Luk, C.; Chan, C. K. Continuous Measurements at the Urban Roadside in an Asian Megacity by Aerosol Chemical Speciation Monitor (ACSM): Particulate Matter Characteristics during Fall and Winter Seasons in Hong Kong. *Atmos. Chem. Phys.* **2016**, *16*, 1713−1728.

(53) Zheng, M.; Fang, M.; Wang, F.; To, K. L. Characterization of the Solvent Extractable Organic Compounds in PM2.5 Aerosols in Hong Kong. *Atmos. Environ.* **2000**, *34*, 2691−2702.

(54) Cochran, R. E.; Laskina, O.; Jayarathne, T.; Laskin, A.; Laskin, J.; Lin, P.; Sultana, C.; Lee, C.; Moore, K. A.; Cappa, C. D.; et al. Analysis of Organic Anionic Surfactants in Fine and Coarse Fractions of Freshly Emitted Sea Spray Aerosol. *Environ. Sci. Technol.* **2016**, *50*, 2477−2486.

(55) He, L.-Y.; Hu, M.; Huang, X.-F.; Yu, B.-D.; Zhang, Y.-H.; Liu, D.-Q. Measurement of Emissions of Fine Particulate Organic Matter from Chinese Cooking. *Atmos. Environ.* **2004**, *38*, 6557−6564.

(56) Schauer, J. J.; Kleeman, M. J.; Cass, G. R.; Simoneit, B. R. T. Measurement of Emissions from Air Pollution Sources. 4. C1-C27 Organic Compounds from Cooking with Seed Oils. *Environ. Sci. Technol.* **2002**, *36*, 567−575.

(57) Zhao, Y.; Hu, M.; Slanina, S.; Zhang, Y. Chemical Compositions of Fine Particulate Organic Matter Emitted from Chinese Cooking. *Environ. Sci. Technol.* **2007**, *41*, 99−105.

(58) Feng, J.; Chan, C. K.; Fang, M.; Hu, M.; He, L.; Tang, X. Impact of Meteorology and Energy Structure on Solvent Extractable Organic Compounds of PM2.5 in Beijing, China. *Chemosphere* **2005**, *61*, 623−632.

(59) Pleik, S.; Spengler, B.; Schäfer, T.; Urbach, D.; Luhn, S.; Kirsch, D. Fatty Acid Structure and Degradation Analysis in Fingerprint. *J. Am. Soc. Mass Spectrom.* **2016**, *27*, 1565−1574.

(60) Cheng, Y.; Li, S. M.; Leithead, A.; Brickell, P. C.; Leaitch, W. R. Characterizations of Cis-Pinonic Acid and n-Fatty Acids on Fine Aerosols in the Lower Fraser Valley during Pacific 2001 Air Quality Study. *Atmos. Environ.* **2004**, *38*, 5789−5800.

(61) USEPA Exposure and Risk Assessment For Benzo a Pyrene and Other Polycyclic Aromatic Hydrocarbons. 1982, *Volume IV*.

(62) Velasco, E.; Siegmann, P.; Siegmann, H. C. Exploratory Study of Particle-Bound Polycyclic Aromatic Hydrocarbons in Different Environments of Mexico City. *Atmos. Environ.* **2004**, *38*, 4957−4968.

(63) Liu, D.; Lin, T.; Syed, J. H.; Cheng, Z.; Xu, Y.; Li, K.; Zhang, G.; Li, J. Concentration, Source Identification, and Exposure Risk Assessment of PM2.5-Bound Parent PAHs and Nitro-PAHs in Atmosphere from Typical Chinese Cities. *Sci. Rep.* **2017**, *7*, 1−12.

(64) Zhang, Y.; Tao, S. Global Atmospheric Emission Inventory of Polycyclic Aromatic Hydrocarbons (PAHs) for 2004. *Atmos. Environ.* **2009**, *43*, 812−819.

(65) Lee, J. Y.; Kim, Y. P. Source Apportionment of the Particulate PAHs at Seoul, Korea: Impact of Long Range Transport to a Megacity. *Atmos. Chem. Phys.* **2007**, *7*, 3587−3596.

(66) Cao, J. J.; Zhu, C. S.; Tie, X. X.; Geng, F. H.; Xu, H. M.; Ho, S. S. H.; Wang, G. H.; Han, Y. M.; Ho, K. F. Characteristics and Sources of Carbonaceous Aerosols from Shanghai, China. *Atmos. Chem. Phys.* **2013**, *13*, 803−817.

(67) Wang, Q.; Liu, M.; Yu, Y.; Li, Y. Characterization and Source Apportionment of PM2.5-Bound Polycyclic Aromatic Hydrocarbons from Shanghai City, China. *Environ. Pollut.* **2016**, *218*, 118−128.

(68) He, L.-Y.; Hu, M.; Zhang, Y.-H.; Huang, X.-F.; Yao, T.-T. Fine Particle Emissions from On-Road Vehicles in the Zhujiang Tunnel, China. *Environ. Sci. Technol.* **2008**, *42*, 4461−4466.

(69) Fraser, M. P.; Lakshmanan, K.; Fritz, S. G.; Ubanwa, B. Variation in Composition of Fine Particulate Emissions from Heavy-Duty Diesel Vehicles. *J. Geophys. Res.* **2002**, *107*, 8346.

(70) Rogge, W. F.; Hlldemann, L. M.; Mazurek, M. A.; Caw, G. R.; Simoneit, B. R. T. Sources of Fine Organic Aerosol. 2. Noncatalyst and Catalyst-Equipped Automobiles and Heavy-Duty Diesel Trucks. *Environ. Sci. Technol.* **1993**, *27*, 636−651.

(71) Schauer, J. J.; Kleeman, M. J.; Cass, G. R.; Simoneit, B. R. T. Measurement of Emissions from Air Organic Compounds from Gasoline-Powered Motor Vehicles. *Environ. Sci. Technol.* **2002**, *36*, 1169−1180.

(72) Schauer, J. J.; Kleeman, M. J.; Cass, G. R.; Simoneit, B. R. T. Measurement of Emissions from Air Pollution Sources. 2. C 1 through C 30 Organic Compounds from Medium Duty Diesel Trucks. *Environ. Sci. Technol.* **1999**, *33*, 1578−1587.

(73) Zhang, Y.; Schauer, J. J.; Zhang, Y.; Zeng, L.; Wei, Y.; Liu, Y.; Shao, M. Characteristics of Particulate Carbon Emissions from Real-World Chinese Coal Combustion. *Environ. Sci. Technol.* **2008**, *42*, 5068−5073.

(74) Yu, H. *Size Distributions of Elemental Carbon , Organic Carbon, and Polycyclic Aromatic Hydrocarbons in Ambient Aerosols of the Pearl River Delta Region*. Hong Kong Univeristy Sci. Techanology. 2009.

(75) Gu, Z.; Feng, J.; Han, W.; Wu, M.; Fu, J.; Sheng, G. Characteristics of Organic Matter in PM2.5 from an e-Waste Dismantling Area in Taizhou, China. *Chemosphere* **2010**, *80*, 800−806.

https://dx.doi.org/10.1021/acsearthspacechem.0c00205
ACS Earth Space Chem. 2020, 4, 1670−1685

(76) Paatero, P.; Tapper, U. Positive Matrix Factorization—A Nonnegative Factor Model with Optimal Utilization of Error-Estimates of Datavalues. *Environmetrics* **1994**, *5*, 111−126.

https://dx.doi.org/10.1021/acsearthspacechem.0c00205
ACS Earth Space Chem. 2020, 4, 1670−1685